Conformational Influence of the Ribose 2′-Hydroxyl Group: Crystal Structures of DNA–RNA Chimeric Duplexes†,‡

Martin Egli,*,§ Nassim Usman,⊥ and Alexander Rich

Department of Biology, Massachusetts Institute of Technology, Cambridge, Massachusetts 02139

Received September 17, 1992; Revised Manuscript Received December 23, 1992

ABSTRACT: We have crystallized three double-helical DNA–RNA chimeric duplexes and determined their structures by X-ray crystallography at resolutions between 2 and 2.25 Å. The two self-complementary duplexes [*r*(*G*)d(CGTATACGC)]$_2$ and [d(GCGT)*r*(*A*)d(TACGC)]$_2$, as well as the Okazaki fragment d(GGGTATACGC)·*r*(*GCG*)d(TATACCC), were found to adopt A-type conformations. The crystal structures are non-isomorphous, and the crystallographic environments for the three chimeras are different. A number of intramolecular interactions of the ribose 2′-hydroxyl groups contribute to the stabilization of the A-conformation. Hydrogen bonds between 2′-hydroxyls and 5′-oxygens or phosphate oxygens, in addition to the previously observed hydrogen bonds to 1′-oxygens of adjacent riboses and deoxyriboses, are observed in the DNA–RNA chimeric duplexes. The crystalline chimeric duplexes do not show a transition between the DNA A- and B-conformations. CD spectra suggest that the Okazaki fragment assumes an A-conformation in solution as well. In this molecule the three RNA residues may therefore lock the complete decamer in the A-conformation. Crystals of an all-DNA strand with the same sequence as the self-complementary chimeras show a morphology which is different from those of the chimera crystals. Moreover, the oligonucleotide does not match any of the sequence characteristics of DNAs usually adopting the A-conformation in the crystalline state (e.g., octamers with short alternating stretches of purines and pyrimidines). In DNA–RNA chimeric duplexes, it is therefore possible that a single RNA residue can drive the conformational equilibrium toward the A-conformation.

Hybrids between DNA and RNA play a crucial role in biological information transfer. Two types of hybrid duplexes can be differentiated. In one, formed during transcription of DNA into RNA, the hybrid consists of a homo-DNA and a homo-RNA strand. These duplexes were first studied with synthetic polynucleotides (Rich, 1960). This type of hybrid is also present during reverse transcription of viral RNA sequences into DNA. In the other hybrid type, the duplex contains DNA·RNA[1] hybrid base pairs in one portion of the molecule and normal DNA·DNA base pairs in the rest of the molecule. Such DNA–RNA chimeric duplexes are formed in replication during DNA synthesis of the lagging strand, where a chimeric DNA–RNA strand is paired with an all-DNA strand. Called an Okazaki fragment, it may be viewed as a short DNA·RNA hybrid duplex covalently linked to a DNA·DNA duplex. In replication, one DNA strand is copied continuously (the leading strand), while the complementary template strand is replicated in a discontinuous way since both prokaryotic and eukaryotic DNA polymerases require a 3′-hydroxyl terminus of a primer and cannot initiate new chains de novo (Kornberg, 1974; Okazaki et al., 1967, 1968). This lagging strand is primed by short RNA oligonucleotides laid down by a primase (ca. 10 residues long) and is then elongated by the DNA polymerase [reviewed in Ogawa and Okazaki (1980)].

Okazaki-type DNA·RNA hybrids are substrates for a number of enzymes. In *Escherichia coli*, the lagging strand RNA primer is removed by a 5′–3′ exonuclease activity of DNA polymerase. In eukaryotic cells, RNase H from chick embryos was found to cleave the chimeric strand at the phosphodiester linkage between the RNA primer and the DNA of a poly(dT)·poly(*rA*)–poly(dA) Okazaki fragment (Sawai & Tsukada, 1983). Various enzymes, such as RNase H (Crough & Dirksen, 1983) and the reverse transcriptases, interact very specifically with homo-DNA·homo-RNA hybrids. The reverse transcriptase of human immunodeficiency virus (HIV-1) is essential for the life cycle of the virus (Mitsuya & Broder, 1987; Goff, 1990). The enzyme consists of an N-terminal polymerase domain and a C-terminal RNase H domain (Johnson et al., 1986; Hansen et al., 1988; Tisdale et al., 1988; Schatz et al., 1989). The RNase activity degrades the RNA template of the hybrid during synthesis of viral DNA and is required for HIV-1 replication (Omer & Faras, 1982; Panganiban & Fiore, 1988; Hu & Temin, 1990; Huber & Richardson, 1990; Evans et al., 1991). To understand the mechanisms of enzyme–substrate recognition and the enzyme cleaving mode, it is essential to know the three-dimensional structures of the DNA–RNA hybrid substrates.

The structural features of both types of DNA·RNA hybrids have been the focus of numerous publications. Early fiber diffraction data suggested that the structure of a homo-DNA·homo-RNA hybrid is similar to that of A-DNA (Milman et al., 1967). The diffraction patterns of various homo-polynucleotide DNA·RNA hybrid fibers confirm that

† This research was supported by grants from the National Institutes of Health, the American Cancer Society, the National Science Foundation, the Office of Naval Research, and the National Aeronautics and Space Administration. N.U. was funded by an NIH Fogarty International Research Fellowship.

‡ Atomic coordinates and isotropic temperature factors for the crystal structures have been deposited in the Brookhaven Protein Data Bank, Chemistry Department, Brookhaven National Laboratory, Upton, NY 11973 (entry numbers 1D87 (*G*-chimera), 1D88 (*A*-chimera), and 1OFX (Okazaki fragment).

* Author to whom correspondence should be addressed.

§ New address: Organic Chemistry Laboratory, Swiss Federal Institute of Technology, CH-8092 Zürich, Switzerland.

⊥ New address: Ribozyme Pharmaceuticals Inc., 2950 Wilderness Place, Boulder, CO 80301.

[1] Symbols: A dot (·) indicates a hydrogen-bonded interaction between bases or strands. A dash (–) indicates covalently linked residues within the same strand. Ribonucleotides are in italic type in the text.

0006-2960/93/0432-3221$04.00/0

the A-conformation is the commonest secondary structural type in hybrids (Arnott et al., 1986). However, poly(*rA*)·poly(dT) hybrid diffraction patterns are consistent with a model in which the two strands have different sugar puckers, C2′-endo for the DNA strand and C3′-endo for the RNA strand (Zimmerman & Pheiffer, 1981). The polymorphic behavior of this particular hybrid was confirmed by NMR and Raman experiments (Shindo & Matsumoto, 1984; Gupta et al., 1985; Benevides & Thomas, 1988; Katahira et al., 1990). A high-resolution NMR structure of a homo-DNA·homo-RNA dodecamer duplex also suggested a somewhat heterogeneous behavior of the two strands (Chou et al., 1989). One-dimensional NMR spectra for a homopurine·homopyrimidine Okazaki fragment, $dG_n{\cdot}r(C_{11})dC_{16}$, were consistent with coexisting A- and B-type duplexes, in which the hybrid duplex and the DNA duplex adopt A- and B-conformations, respectively (Selsing et al., 1978). The conformation of the Okazaki fragment was subsequently modeled, and a fully base-paired junction site, spread over three base pairs, was proposed (Selsing et al., 1979). These results, as well as the high-resolution NMR structure of an Okazaki-type hybrid (Fujii et al., 1989), appear to provide evidence against significant propagation of secondary structure along the DNA duplex by the RNA portion.

The findings of structural studies with self-complementary DNA·RNA hybrids are somewhat inconsistent. Some investigations, based on either single-crystal X-ray crystallography, Raman spectroscopy, or solution NMR, support the idea that the conformational characteristics of the hybrid duplex are dominated by the conformational preferences of the RNA component (Wang et al., 1982a; Benevides et al., 1986; Happ et al., 1988). On the other hand, the sugar puckers of DNA residues in self-complementary hybrids (with the DNA residues lying opposite either DNA or RNA residues) were found to deviate from the typical C3′-endo mode expected for A-type conformations (Mellema et al., 1983; Chou et al., 1991). From these results, one can thus conclude that the structures of DNA·RNA hybrids are quite polymorphous and that their conformation may depend on various parameters, such as solvent conditions or base sequence.

We have determined the three-dimensional structures of three DNA–RNA chimeric duplexes by single-crystal X-ray crystallography. We describe the conformations of the duplexes and the role of the ribose 2′-hydroxyls in the stabilization of the particular conformations. A single RNA residue was placed at two different sites within the self-complementary sequence d(GCGTATACGC). In the *G*-chimera $[r(G)d(CGTATACGC)]_2$, the RNA residues are located at the two termini, and in the *A*-chimera [d(GCGT)-$r(A)$d(TACGC)]$_2$, the RNA residues are located at the center of the duplex (see Figure 1A,B). The all-DNA duplex $[d(GCGTATACGC)]_2$ was crystallized to evaluate the conformational influence of the RNA residues, and CD spectroscopy was used to study the conformations adopted by the DNA and the chimeras in solution. The geometry of a junction between a DNA·RNA hybrid duplex and a DNA·DNA duplex, as found in Okazaki fragments, was investigated with a double-helical decamer, composed of the chimeric RNA–DNA strand *r*(*GCG*)d(TATACCC) and the complementary DNA strand d(GGGTATACGC) [Figure 1C, briefly described in Egli et al. (1992)]. This structure allows us to examine the degree of secondary structure propagation along the DNA duplex exerted by a short stretch of RNA.

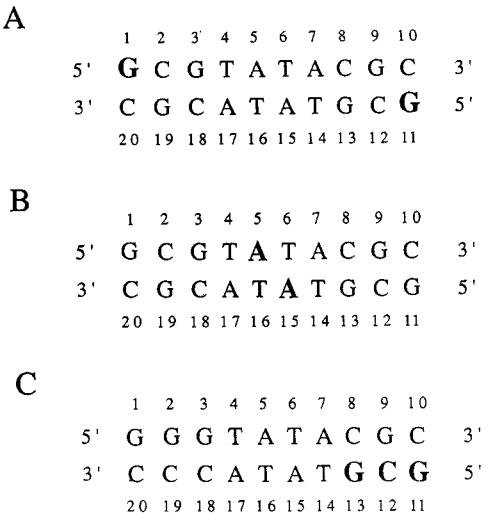

FIGURE 1: Sequences of the DNA–RNA chimeras (RNA residues in larger, bold font): (A) the *G*-chimera, (B) the *A*-chimera, and (C) the Okazaki fragment. In the case of the two self-complementary chimeric decamers, the bases of one strand are numbered 1–10, and the bases of the other are numbered 11–20.

MATERIALS AND METHODS

Chimeric Duplex Synthesis, Purification, and Crystallization. Preparation and crystallization of the DNA–RNA chimera strands have been described elsewhere in detail (Egli et al., 1992; Usman et al., 1992). The sequences and the numbering scheme for the strands are shown in Figure 1.

Data Collection and Reduction. Crystallographic cell constants and space groups for all three structures were determined from precession photographs. Crystals with approximate dimensions 0.5 × 0.4 × 0.3 mm^3 (*G*-chimera) and 0.8 × 0.5 × 0.2 mm^3 (*A*-chimera) were sealed in capillaries with a droplet of mother liquor and mounted on a four-circle diffractometer (Rigaku AFC5R), equipped with a rotating copper anode and a graphite monochromator ($\lambda_{CuK\alpha}$ = 1.5406 Å). The temperatures for data collection were 0 °C for the *G*-chimera and 2 °C for the *A*-chimera. In both cases, the crystallographic cells were refined with reflections in a 2θ range between 11° and 16°. Reflections were then measured by the ω-scan method (scan speed 4°/min), and decay of the crystals was checked with three reflections in different 2θ ranges. The average decays in both cases were well below 10%. Crystal data, reflection statistics, and resolution in Å for the three hybrids are listed in Table I. In the case of the Okazaki fragment, data of three different crystals were collected at room temperature, 10 °C, and −110 °C (Egli et al., 1992). Data were corrected for Lorentz and polarization effects. A semiempirical absorption correction based on Ψ scans for two or three reflections with χ values higher than 85° was applied in all three cases (North et al., 1968).

Structure Solution and Refinement. The space group of all three hybrid crystals is orthorhombic $P2_12_12_1$. The differences between the dimensions of their cells are considerable, however, and indicate that the three structures are non-isomorphous (Table I). The crystal structures were determined by the molecular replacement method, using an A-type conformation trial structure (Wang et al., 1982a) with the rotation/translation search program ULTIMA (Rabinovich & Shakked, 1984). The orientations of the duplexes within their respective crystallographic unit cells are shown in Figure 2. As is visible from the panels in the right column (projections along the crystallographic *x*-axes), the orientations and, therefore, the crystallographic environments of the duplexes

Table I: Crystal Data and Selected Crystallographic Refinement Parameters

parameter	G-chimera	A-chimera	Okazaki fragment
cell constants (Å)			
a	27.50	25.25	24.03, 24.82[a]
b	44.23	45.73	43.67, 45.22[a]
c	44.61	45.83	48.95, 47.92[a]
space group	$P2_12_12_1$	$P2_12_12_1$	$P2_12_12_1$
total non-hydrogen atoms	513	500	514
DNA non-hydrogen atoms	406	406	407
cation and water non-hydrogen atoms	107	94	107
no. of $F_o > 2\sigma(F_o)$	1592	2285	1826
resolution (Å)	2.25	2.0	2.0
total no. of variables [(no. of atoms) × 4, plus overall scale factor]	2053	2001	2056
overdeterminancy ratio (F_o/variables)	0.8	1.1	0.9
total no. of restraints (bond length, bond angles, planar groups, chiral volumes, van der Waals contacts)	3326	3326	3337
data:restraint ratio	0.5	0.7	0.6
final *R* factor (%)	17.8	19.5	15.6
final weight (w)[b] on structure factors	17.5	15	17.5
average $\|F_o - F_c\|$ for all reflections	31.7	24.5	25.5
RMS deviations from ideal bond lengths (Å)[c]	0.02	0.02	0.02
RMS deviations from planes (Å)	0.01	0.01	0.01
RMS deviations of chiral volumes (Å^3)	0.14	0.14	0.13
RMS deviations from minimal van der Waals distances (Å)			
separated by two bonds	0.17	0.17	0.16
separated by more than two bonds or nonbonded	0.19	0.18	0.16

[a] Room temperature. [b] The minimized weighted function Φ_F for structure factors is $\Phi_F = \sum_{i=1}^{n(obsd)} (1/w)^2(|F_o(i)| - F_c(i)|)^2$. [c] Hendrickson and Konnert (1981).

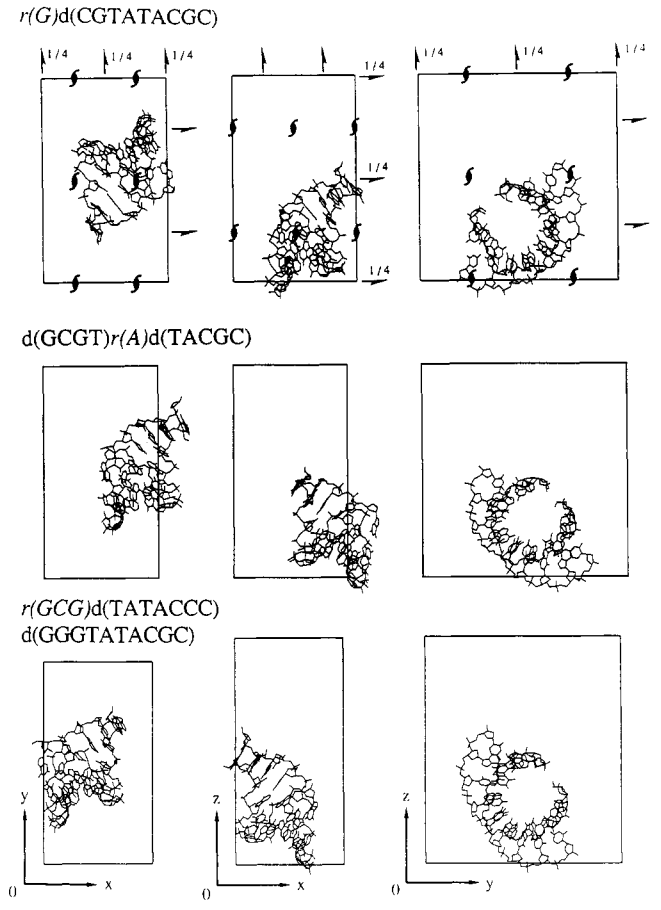

FIGURE 2: Orientation of *G*-chimera (top), *A*-chimera (middle), and Okazaki fragment (bottom) in their respective lattices. The three columns show projections along the crystallographic *z*-axes (left), *y*-axes (center), and *x*-axes (right). The space group in all three cases is orthorhombic $P2_12_12_1$, and symbols for the crystallographic symmetry elements have been included in the projections of the *G*-chimera cell.

are distinct in the three cases. The orientations are also different from the one determined for a self-complementary DNA–RNA chimeric duplex by Wang et al. (sequence [*r*(*GCG*)d(TATACGC)]$_2$, space group $P2_12_12_1$). The rotational/translational searches were typically performed with a restricted number of reflections (between 25- and 8-Å resolution) at the beginning, using relatively rough search grids of 15° (rotational degrees of freedom) and 1.5 Å (translational degrees of freedom) within the asymmetric unit of the search space (Hirshfeld, 1968). The resolution range was then extended in 1-Å steps, and rigid body refinements were used to a resolution of 3 Å (the low-resolution limit was 10 Å) with refined search grids. For the three structures, the *R* factors of structure factor calculations with models refined in the above way were between 42 and 45%. The *R* factors of the second-best solutions were usually 5% higher.

Atomic positions and isotropic temperature factors were refined with 3-Å data using the Konnert–Hendrickson least-squares procedure (Hendrickson & Konnert, 1981) as modified for nucleic acids (Quigley et al., 1978) with relatively stringent stereochemical restraints. For the Okazaki fragment, the orientation of the duplex with respect to its pseudo-2-fold rotation axis (see Figure 1) was still ambiguous at this point. The determination of the correct orientation, as well as the degree of disorder present, has been described elsewhere in detail (Egli et al., 1992). Initial refinements of the self-complementary chimera structures were performed with all-DNA duplexes. As more data were included in the refinement, the structure factors were weighted more heavily, and at full resolution (Table I), Fourier electron sum- ($2F_o - F_c$) and difference-density maps ($F_o - F_c$) were displayed on an Evans and Sutherland (Salt Lake City) PS 390 graphics terminal with the program FRODO (Jones, 1978). Positions of water and spermine (Okazaki fragment) molecules were determined from sum- and difference-density maps and were included in the refinement together with the 2′-hydroxyls of the ribose residues. Table I lists selected refinement parameters, final *R* factors, and deviations from ideal parameters for the three chimera structures. The final asymmetric unit contained the duplex and 107 water molecules (*G*-chimera); the duplex and 94 water molecules (*A*-chimera); and the duplex, 93 water molecules, and one spermine molecule (Okazaki fragment).

CD Spectroscopy. Oligonucleotide concentrations were 10 μM (ca. 3.3 μg/mL) for the comparisons between the spectra of the all-DNA duplex and the three hybrid duplexes (Figure 13B) and 50 μM for the spectra of the all-DNA duplex and the all-RNA duplex (Figure 13A). In all cases, the buffer was sodium cacodylate (pH 7), and the solutions contained 100 mM sodium chloride and 5 mM magnesium chloride. Spectra were measured five times on an AVIV CD spectrometer (Model 60 DS) at 2 °C between 300 and 210 nm and then averaged. The wavelength step size was 0.5 nm, with an equilibration time of 2 s.

RESULTS

Overall Conformation of G- and A-Chimeric Duplexes. Both chimeras adopt an A-type conformation. The *G*-chimera has 11.3 residues per turn, and the *A*-chimera has 10.8 residues per turn. The structures deviate somewhat from a regular A-conformation duplex with 11 residues per turn and are also different from each other. The duplexes exhibit the normal features of the A-conformation, such as inclined base pairs with respect to the helical axis and large propeller twists of the bases. Propeller twist is a rotation of bases around their long axes (Watson–Crick hydrogen-bonding direction) relative to each other. The average inclination of base pairs relative to the helical axis is 17(4)° for the *G*-chimera and 19(3)° for the *A*-chimera (standard deviations in parentheses). The average propeller twists are −15° for both chimeric duplexes with standard deviations of 6° and 7° for the *G*- and the *A*-chimera, respectively.

Notable features, which both chimeras share, are the large values for base roll between base pairs T(4)·A(17) and A(5)·T(16) and between base pairs T(6)·A(15) and A(7)·T(14) (see residue numbering in Figure 1; in the case of the *A*-chimera, A(5) and A(15) are RNA residues). The roll values for these two base pairs in the *G*-chimera are 19° and 22° (cf. the duplex average value of 8°). In the *A*-chimera, the two rolls are 20° and 19° (the duplex average value is 9°). The base rolls between the central base pairs A(5)·T(16) and T(6)·A(15) are lower, however, in both the *G*-chimera, 9°, and the *A*-chimera, 2° (in the case of the *A*-chimera, A(5) and A(15) are RNA residues). The large base rolls are accompanied by an unwinding of the helices and a partial unstacking of bases at the above steps. Helical twist and rise values for the two chimeric duplexes are listed in Table II, sections A and B. The average helical twist for both is 33°, and the average rises are approximately 2.5 Å. For both pyrimidine–purine TpA steps in the duplexes, the values for twist are lower than the average (*G*-chimera, 22° and 27°; *A*-chimera, 26° and 30°). Similarly, the values for rise at the two steps are larger than the average (*G*-chimera, 3.3 and 2.6 Å; *A*-chimera, 2.8 and 2.6 Å). Both chimeric duplexes are slightly overwound at their central step, with helical rises close to the average value. The duplexes thus adopt nonuniform geometries with some local deviations, indicating significant sequence dependencies of the A-conformation.

Groove topologies constitute a fundamental difference between the DNA A- and B-conformations. In B-DNA, the arrangement of the sugar–phosphate backbones generates a wide and relatively shallow major groove and a narrow minor groove. However, in A-DNA the topology is reversed: the major groove is narrow and very deep, and the minor groove is wide and shallow. Space-filling representations for *G*- and *A*-chimeric duplexes are shown in Figures 3 and 4, respectively. The differences between the grooves in A-type conformations can easily be seen from views across the major and the minor grooves of the duplexes, shown in Figures 3B and 4B. In Figure 3B, the deep major groove opens to the left, and the minor groove opens to the right. In Figure 4B, the view is in the opposite direction, and the major groove opens to the right. In the *G*-chimera the average width of the major groove is 6.2 Å, and that of the minor groove is 9.8 Å (phosphorus–phosphorus distances less 5.8 Å, the sum of the van der Waals radii of two phosphate groups). In the *A*-chimera both grooves are slightly narrower, with widths of 5.7 and 9.7 Å. In both duplex chimeras, the major grooves are slightly wider at the central base pairs. The 2′-hydroxyls of the RNA residues in both duplexes are located at the borders of the minor groove. This can be seen in Figure 3 for the *G*-chimera. In Figure 3A, the minor groove is situated at the top and at the bottom, running behind the molecule from the upper left to the lower right. The 2′-hydroxyls (red) of RNA residues *rG*(1) and *rG*(11) (purple) are directed away from the bases, lying close to the surface of the duplex. In Figure 3B, the two 2′-hydroxyls appear as red spheres on the left side of the duplex, pointing to the outside. A similar situation is found in the *A*-chimera. In Figure 4A, the view is into the minor groove, and the 2′-hydroxyls (red) of RNA residues *rA*(5) and *rA*(15) (purple) are lying on opposite sides of the groove, embedded in the sugar–phosphate backbone. In the view across the grooves shown in Figure 4B, the two 2′-hydroxyls appear as red spheres on the left side of the duplex, pointing to the outside. Thus, the 2′-hydroxyls are lying close to the surface of the shallow groove in the A-conformation and can be readily probed by molecules interacting with the chimeric duplexes, such as the side chains of proteins.

Overall Conformation of the Okazaki Fragment. The duplex adopts a fairly regular A-type conformation with 11.1 residues per turn. The average inclination of base pairs relative to the helix axis is 19(3)°, and the average propeller twist between paired bases is −14(5)° (standard deviations in parentheses). Selected helical parameters for the Okazaki fragment are listed in Table II, section C. The particular arrangements of base pairs T(4)·A(17) and A(5)·T(16), as well as of T(6)·A(15) and A(7)·T(14), relative to each other, which were already observed with the *G*- and *A*-chimeras, are also present in the structure of the Okazaki fragment. The roll between the former base pairs is 25°; between the latter ones, 20°. Both rolls are larger than the average value of 8° and constitute the largest rolls between base pairs in the duplex. Also, the duplex is slightly underwound at the two steps. The helical twists at the above steps are 28° and 30°, the lowest values found for the duplex and both considerably smaller than the average value of 33°. The higher helical rises at these sites (2.9 and 2.7 Å; average value 2.5 Å) are a further indication of partial unstacking of the bases at the two TpA steps. As in the case of the self-complementary chimeras, the central base pairs A(5)·T(16) and T(6)·A(15) show no peculiarities in their relative rolls (3°), twists (33°), and rises (2.6 Å).

An Okazaki fragment consists of a chimeric RNA–DNA molecule base-paired to an all-DNA strand to form a hybrid RNA·DNA duplex contiguous to a DNA·DNA duplex. The former is normally associated with an A-type conformation, whereas the B-type conformation is most common for the latter. An analysis of the helical parameters shows no evidence for a conformational transition between the DNA·RNA hybrid *r*(*GCG*)-d(CGC) portion and the double-helical DNA heptamer d(TATACCC)·d(GGGTATA) portion. As reported earlier, some base pairs in the hybrid section or within the junction show considerable perturbations, such as buckling

Table II: Backbone and Glycosyl Torsion Angles, Selected Helical Parameters, and Sugar Conformations for the Three Chimeric Duplexes[a]

residue	α	β	γ	δ	ε	ζ	χ	rise (Å)	twist (Å)	sugar pucker
					A. *G*-Chimera					
rG1			18	101	−168	−81	−160	2.43	33.6	C2′-exo
C2	159	−126	156	73	−92	−108	174	2.19	26.7	C3′-endo
G3	−57	94	96	72	−162	−58	161	2.05	47.4	C3′-endo
T4	−115	−145	54	60	167	−26	−129	3.32	21.8	C3′-endo
A5	122	−163	−178	63	153	3	−168	2.74	37.3	C2′-exo
T6	−157	−167	95	76	−126	−83	−157	2.61	27.4	C2′-exo
A7	−28	146	33	65	150	−5	−175	1.87	35.3	C3′-endo
C8	−37	144	27	78	−167	−68	−153	1.91	32.6	C4′-exo
G9	−90	156	64	63	−155	−91	−172	3.18	36.3	C3′-endo
C10	0	170	−6	91			−159			C2′-exo
rG11			85	91	−172	−76	−173			C2′-exo
C12	147	−123	167	96	−136	−49	−152			C3′-endo
G13	−92	121	112	57	−136	−85	167			C4′-exo
T14	−17	−177	0	77	157	−12	−145			C2′-exo
A15	−164	−162	99	94	−168	−136	−174			C3′-endo
T16	68	77	23	56	−145	−86	−174			C3′-endo
A17	−25	162	23	81	177	−63	−150			C3′-endo
C18	96	176	−130	88	145	36	−152			C2′-exo
G19	−162	128	110	94	−113	−92	−175			C2′-exo
C20	28	−135	−73	106			−145			C1′-endo
average[b]	87	143	77	79	149	64	161	2.48	33.1	
SD	56	28	54	15	22	37	13	0.53	7.4	
					B. *A*-Chimera					
G1			127	99	−136	−69	−165	2.60	38.1	C2′-exo
C2	−76	170	62	69	171	−28	−156	1.90	29.7	C3′-endo
G3	−117	−178	84	79	−173	−49	−165	2.75	37.4	C3′-endo
T4	−92	−165	48	80	−138	−37	−143	2.81	25.8	C3′-endo
rA5	−56	177	39	72	−173	−49	−161	2.73	35.1	C3′-endo
T6	−163	164	134	91	−119	−87	−169	2.63	30.3	C2′-exo
A7	−32	144	16	66	−169	−99	−149	2.24	33.0	C3′-endo
C8	21	120	−5	73	162	−64	−150	2.18	35.4	C3′-endo
G9	−156	−144	115	71	−145	−67	−176	2.81	32.2	C3′-endo
C10	−64	−171	56	84			−151			C3′-endo
G11			102	90	−109	−67	177			C2′-exo
C12	−99	121	113	87	−111	−99	−170			C2′-exo
G13	−18	132	30	70	−151	−73	−170			C3′-endo
T14	−43	−178	35	87	−138	−63	−157			C2′-exo
rA15	−49	−172	33	104	−154	−100	−157			C2′-exo
T16	2	134	10	80	−144	−96	−144			C3′-endo
A17	59	−151	−105	90	−122	−68	−162			C2′-exo
C18	−75	164	66	81	−150	−72	−174			C3′-endo
G19	−50	158	55	94	−143	−99	−173			C3′-endo
C20	−8	−208	13	72			−148			C3′-endo
average[b]	66	158	62	82	144	71	161	2.52	33.0	
SD	46	23	41	11	20	22	11	0.33	4.0	
					C. Okazaki Fragment					
G1			−137	93	−115	−71	170	2.28	35.6	C2′-exo
G2	−28	168	19	71	158	−21	−164	2.22	34.2	C3′-endo
G3	−102	−165	55	69	−178	−47	−157	2.76	33.1	C3′-endo
T4	−79	−176	50	68	−151	−75	−149	2.94	28.2	C3′-endo
A5	−20	159	22	89	−166	−62	−150	2.60	33.7	C3′-endo
T6	−65	−175	45	87	−158	−82	−146	2.66	30.4	C3′-endo
A7	−26	155	23	87	−177	−75	−146	2.33	31.4	C3′-endo
C8	−67	−175	58	82	−172	−64	−148	2.04	36.3	C3′-endo
G9	−91	171	73	71	−135	−72	−168	2.63	35.3	C3′-endo
C10	−67	159	65	88			−164			C3′-endo
rG11			142	161	−172	−118	−116			C3′-exo
rC12	−62	157	47	71	−158	−69	−148			C3′-endo
rG13	−37	170	16	94	−130	−89	−176			C2′-exo
T14	−48	136	60	66	−132	−83	−175			C3′-endo
A15	−25	154	26	85	−155	−64	−153			C3′-endo
T16	−50	−176	21	87	−176	−38	−148			C2′-exo
A17	−104	176	69	80	−140	−102	−168			C3′-endo
C18	−24	133	41	72	−173	−56	−154			C3′-endo
C19	−171	170	139	82	−143	−74	−179			C2′-exo
C20	−45	168	42	91			−163			C3′-endo
average[b]	62	164	58	85	155	70	157	2.50	33.1	
SD	38	13	39	20	19	22	15	0.29	2.7	

[a] Calculated with the program NEWHELIX [version NEWHEL90 (Dickerson et al., 1989)]. Torsion angles are defined as O3′–P–α–O5′–β–C5′–γ–C4′–δ–C3′–ε–O3′–ζ–P–O5′. [b] Calculated with absolute numbers.

and shearing of bases (Egli et al., 1992). The values for buckle in the case of base pairs A(7)·T(14) and C(8)·*rG*(13) are −13° and −17°, respectively (average of absolute values: 7°). The buckle of the adjacent base pair G(9)·*rC*(12) is positive,

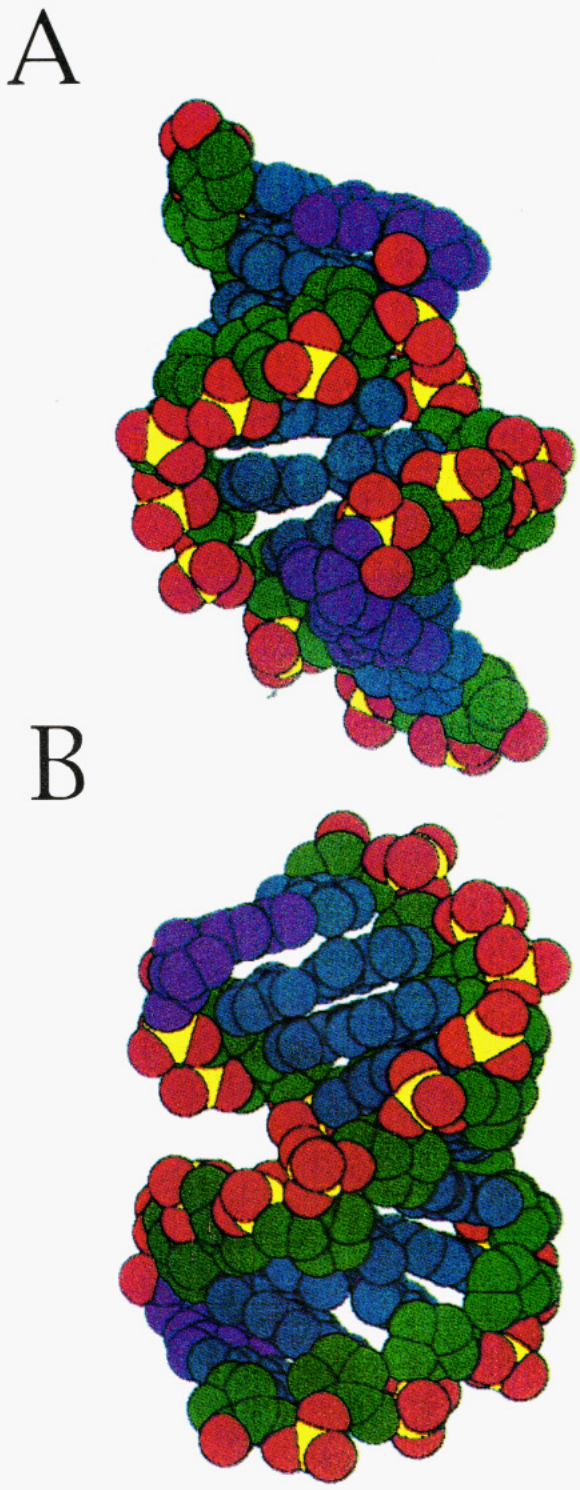

FIGURE 3: van der Waals representations of the *G*-chimera: (A) view into the major groove and (B) view across major (top) and minor (bottom) grooves. van der Waals radii were somewhat reduced for clarity. Phosphorus atoms are yellow, and phosphate oxygens and O3′ and O5′ of the DNA residues, as well as the 2′-oxygens of RNA residues *rG*(1) and *rG*(11), are red. Sugars are green, base atoms are blue, and RNA residues are purple. The drawings in Figures 3–5 were generated on a MacIntosh II, using the program MoMo (Dobler, 1992).

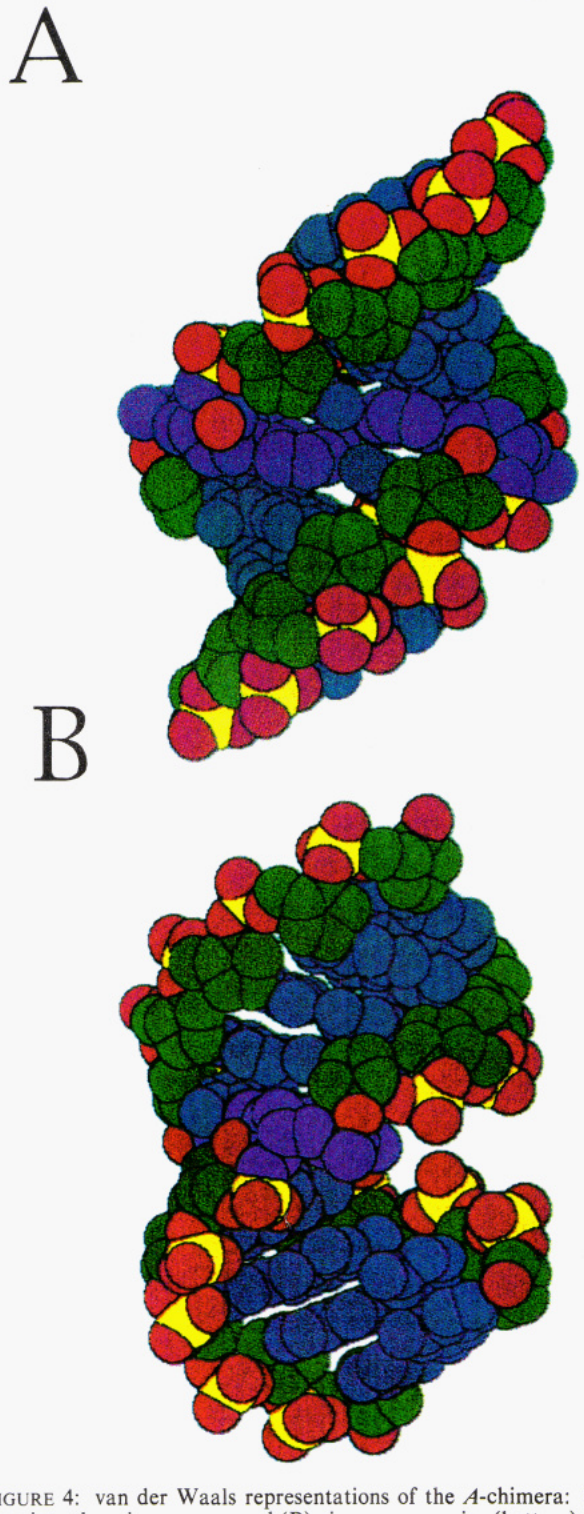

FIGURE 4: van der Waals representations of the *A*-chimera: (A) view into the minor groove and (B) view across major (bottom) and minor (top) grooves. For color coding, see Figure 3.

and the difference between buckles of neighboring base pairs [defined as the parameter cup (Yanagi et al., 1990)] is therefore exceptionally high at this step in the hybrid portion (24°). The largest roll, with the exception of the ones in the two TpA steps described above, is also found at this step within the duplex (10°). The hydrogen-bond geometries of base pairs in the hybrid duplex *r*(*GCG*)·d(CGC) are different from those in the DNA duplex d(GGG)·d(CCC) at the other end of the Okazaki fragment. The terminal base pairs G(9)·*rC*(12) and C(10)·*rG*(11) display considerable amounts of shearing of ~1 Å. Thus, these bases have been displaced from one another in opposite directions within the plane of the base pair, in a direction normal to the Watson–Crick hydrogen bonds. This leads to formation of three-centered hydrogen bonds where, for example, nitrogen N2 of residue *rG*(11) donates to both O2 and N3 of residue C(10).

Two van der Waals representations of the Okazaki fragment are depicted in Figure 5. The two photographs show views of the hybrid across the major and the minor groove from

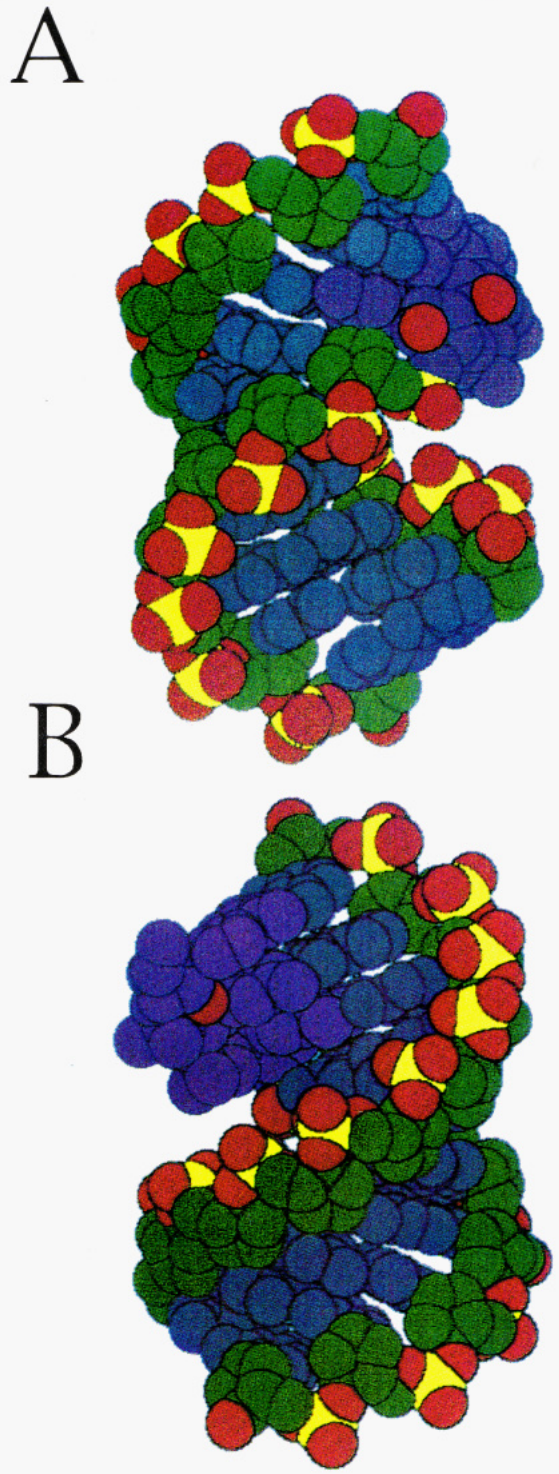

FIGURE 5: van der Waals representations of the Okazaki fragment: (A) view into the minor groove of the hybrid portion of the duplex (major groove at the bottom) and (B) view from the opposite side, into the major groove of the hybrid portion of the duplex (minor groove at the bottom). For color coding, see Figure 3.

opposite directions. In Figure 5A, the major groove opens to the right, and in Figure 5B, it opens to the left. The average width of the major groove is 6.2 Å, and that of the minor groove is 9.8 Å. Two of the 2′-hydroxyls [residues *rC*(12) and *rG*(13)] line the minor groove, lying close to the surface (Figure 5A). The 2′-hydroxyl of residue *rG*(11) forms a hydrogen bond to one of the phosphate oxygens from the adjacent residue. The ribose of the former residue is rotated away, and its 2′-hydroxyl is located in the major groove (Figure 5B). Both ribose 2′-hydroxyls in the minor groove point to the outside and may be contacted by functional groups of molecules interacting with the Okazaki fragment. The altered backbone conformation at residue *rG*(11), which rotates the 2′-hydroxyl into the major groove, may be attributed to the terminal location of this residue.

Backbone Conformation. The geometry of the oligonucleotide backbone from one phosphorus atom to the next can be described with six torsion angles, α–ζ. The torsion angles are defined and listed in Table II for all three chimeric duplexes. Because of the large range, the average angle values were calculated with absolute numbers. Instead of a description of the backbone conformation with numbers, a qualitative description based on the conformational ranges gauche$^+$ (g^+), gauche$^-$ (g^-), and trans (t) of the individual torsion angles may be used. In this description, the most common backbone genus in the case of A-DNA (and A-RNA) has the conformation ($g^-tg^+g^+tg^-$). The angles α and γ show the largest variation in the three chimeric duplexes (with values falling within all three conformational ranges), and in general, the backbone to the 5′ side of the sugar is much more flexible than the riboses, the deoxyriboses (torsion angle δ), or the backbone to the 3′ side of the sugar. An increase in α is associated with a decrease in γ. For the *G*-chimera, only about one-half of the α,γ pairs fall into the expected g^-g^+ angle range. The flexibility of the backbone in the case of the *G*-chimera is also indicated by the large standard deviations from the mean angles. Torsion angles β vary less, with the exception of two cases lying in the g^+ range (*G*-chimera).

Figure 6 shows the superposition of the backbones from paired strands of the *G*- and *A*-chimeras. All atoms were weighted equally, and the complete backbones were included in the superpositions (Kabsch, 1978). Although there are local variations in certain torsion angles, the overall shapes of the strands are similar. As indicated by the torsion angles in Table II, the superposition of the *G*-chimera backbones shows more pronounced local deviations than the one of the *A*-chimera backbones (Figure 6A, backbone area around residues T(4) and A(5) or *rA*(5) of one strand and residues T(14) and A(15) or *rA*(15) of the other, 5′-termini at the top). However, a portion of the larger variations seen in the case of the *G*-chimera may be attributed to the lower resolution of the *G*-chimera structure.

Torsion angle δ is defined around the C3′–C4′ bond and is therefore related to the sugar conformation. The deoxyriboses in A-DNA and the riboses in A-RNA commonly adopt C3′-endo conformations (with δ lying in the g^+ range). Although this conformation is adopted by most of the sugars in the three chimeric duplex structures, there are a number of riboses and deoxyriboses with alternative puckering modes. The sugar puckers for all residues are listed in Table II, and plots for pseudorotation phase angles P and torsion angles δ for the three hybrids are depicted in Figure 7. The diagrams show that deviations from the expected sugar puckering mode (C3′-endo) cannot be attributed to the terminal location of such residues alone. The most obvious deviation is found at residue *rG*(11) for the Okazaki fragment, where the ribose has a C3′-exo conformation (Table II, section C; Figure 7). The adoption of this pucker is related to the formation of a hydrogen bond between the ribose 2′-hydroxyl and a phosphate oxygen from the adjacent residue *rC*(12). In the case of the *A*-chimera the ribose of residue *rA*(15) within the second strand shows a C2′-exo pucker. Its 2′-hydroxyl forms a strong hydrogen bond to the 1′-oxygen of the adjacent residue T(16). The 2′-hydroxyl of the pseudosymmetrical residue *rA*(5) is hydrogen bonded to the 5′-oxygen of residue T(6). The deoxyribose of the latter residue adopts a C2′-exo conformation as well (Table II, section

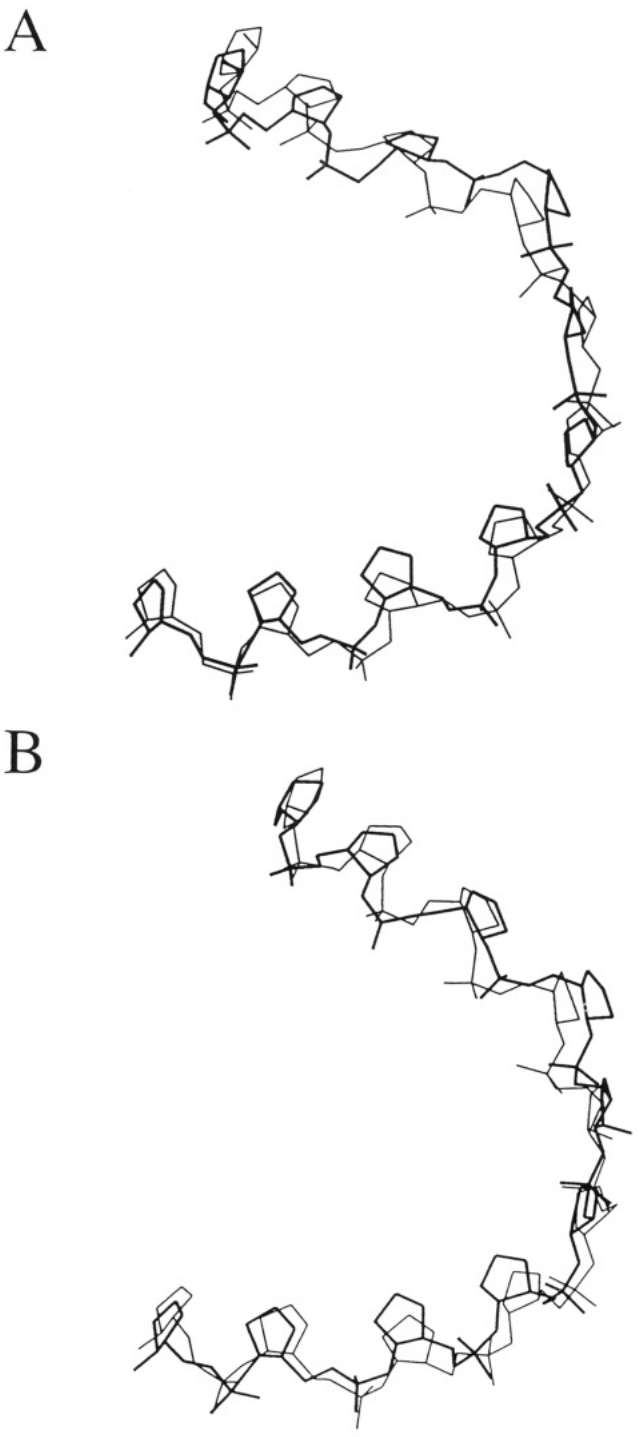

FIGURE 6: Superposition of backbone atoms of strands 1 and 2 for (A) the *G*-chimera and (B) the *A*-chimera. Strand 1 (residues 1–10) is bold, and the RMS deviations between strands are 0.64 Å for the *G*-chimera and 0.47 Å for the *A*-chimera.

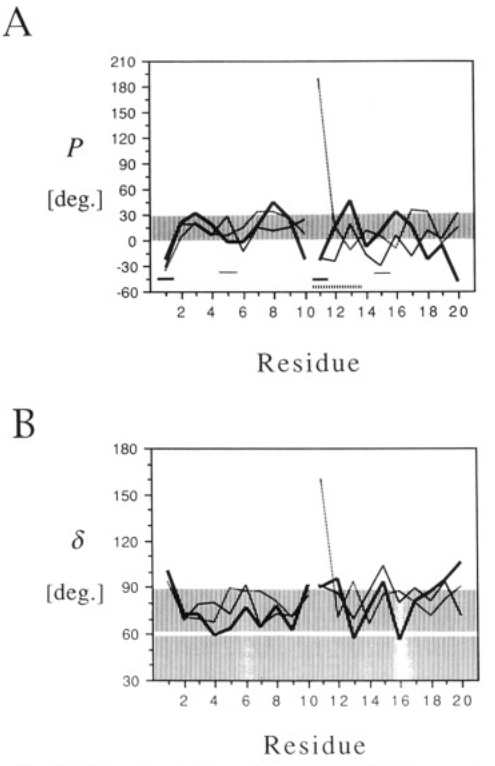

FIGURE 7: (A) Pseudorotation phase angles P of deoxyriboses and riboses in strands 1 and 2 for the *G*-chimera (thick line), the *A*-chimera (thin line), and the Okazaki fragment (dashed line). The angle range normally covered by riboses is shaded in gray. The locations of the RNA residues within the chimeric strands are marked by the short horizontal lines. The pseudorotation phase angle, P, is calculated from the five endocyclic sugar torsion angles ν_i: $\tan P = [(\nu_4 + \nu_1) - (\nu_3 + \nu_0)]/[2\nu_2(\sin 36° + \sin 72°)]$. (B) Torsion angles δ of deoxyriboses and riboses in strands 1 and 2 for the *G*-chimera (thick line), the *A*-chimera (thin line), and the Okazaki fragment (dashed line). The angle range observed with g^+ conformations (horizontal white line in shaded area) is shaded in gray.

B; Figure 7). C1′-endo, C4′-exo, and C2′-exo puckers are direct neighbors of the C3′-endo mode in the furanose pseudorotation cycle. It is important, though, that the A-conformation can accomodate a range of sugar conformations without dramatically altering its overall shape. For the *A*-chimera and the Okazaki fragment, deviations from the standard sugar conformation can be attributed to specific intramolecular contacts of the ribose 2′-hydroxyls.

Phosphorus–phosphorus distances are influenced mostly by the conformation of the sugars. However, the presence of various sugar puckers in the chimeric duplexes does not lead to large deviations in the distances between adjacent phosphorus atoms, and most of them lie within the range of 5.5–6.5 Å expected for A-type conformations. For the *G*-chimera, the average distance is 6.1(0.7) Å, with a short contact of 4.7 Å between phosphorus atoms P4 and P5 and a relatively long distance of 7.3 Å between P5 and P6 of the same strand. As in the case of the other helical parameters, the P···P distances for the *A*-chimera and the Okazaki fragment vary less, and the average value is 5.9 Å for both (with standard deviations of 0.4 and 0.3 Å for the *A*-chimera and the Okazaki fragment, respectively). Most of the glycosyl torsion angles fall into the expected anti range, and the average value is ~160° for all three hybrids, with standard deviations between 10° and 15° (Table II). For some of the RNA residues or residues adjacent to them, the glycosyl torsion angles fall into the anticlinal range. The most dramatic change is observed with residue *rG*(11) in the Okazaki fragment, where the glycosyl torsion angle is compressed to −116°. Such adjustments are probably associated with alterations of backbone torsion angles. Changing α and γ in opposite directions leads to roughly parallel motions of adjacent base pairs. The most likely cause for coupled adjustments of backbone torsion angles and rotations around the glycosidic bond is the improvement of base stacking.

Base-Pair Geometry in the TATA Section. The geometrical features of TpA steps, such as lower helical twists and higher rolls, were mentioned above. In addition, the bases of T·A base pairs in the central part of the *A*-chimera and the Okazaki fragment duplexes are displaced along each other within the plane defined by the base pair (shearing). The combination

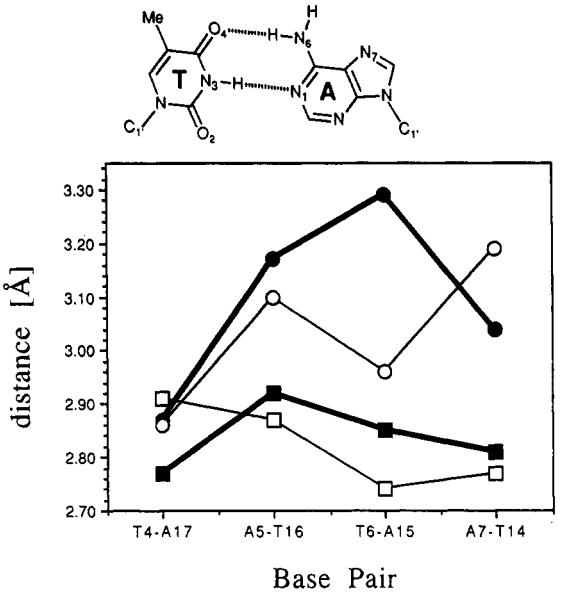

FIGURE 8: (Top) T·A base pair. (Bottom) Plot of hydrogen-bonding distances in the central T·A base pairs of the *A*-chimera (open symbols) and the Okazaki fragment (solid symbols). The combination of roll between base pairs and propeller twist and shearing (sliding of bases relative to each other in a direction normal to Watson–Crick-type hydrogen bonds) between paired bases results in an elongation of O4(thymine)–N6(adenine) hydrogen bonds (circles) compared to N3(thymine)–N1(adenine) hydrogen bonds (squares).

of these adjustments leads to an elongation of the O4-(thymine)–N6(adenine) hydrogen bond relative to the N3-(thymine)–N1(adenine) hydrogen bond. The T·A base pair and a distance plot are shown in Figure 8. The shearing of bases, as well as the reduced twists and higher rolls, can improve the intrastrand stacking between thymines and adenines. Moreover, TpA steps in A-type duplexes exhibit partial interstrand stacking of purine bases, which can be optimized by shearing motions. At GpT or ApC steps, shearing of bases can help to avoid the overlap between keto groups of adjacent guanine (O6) and thymine (O4) bases in the major groove. Alterations in the base-pair geometry also change the topology of the grooves. Depending on the relative motion, the functional groups of either thymine (keto O4 and methyl C5) or adenine (amino N6) are shifted into the major groove. In the latter case, the 2-oxygen of thymine may become more exposed in the minor groove.

Interactions of the Ribose 2′-Hydroxyls. On the basis of the different locations of RNA residues within the three chimeric duplexes, and because of distinct orientations of the duplexes in their crystallographic unit cells, various intramolecular and intermolecular contacts of ribose 2′-hydroxyls are observed in the crystal structures. The interactions of 2′-hydroxyls in the Okazaki fragment structure have been described elsewhere (Egli et al., 1992). Distances of hydrogen bonds formed by 2′-hydroxyls for all three structures and hydrogen-bond partners are listed in Table III. Stereo diagrams of the environments of RNA residues for the *G*- and *A*-chimeras are shown in Figures 9 and 10, respectively.

Intermolecular hydrogen bonds between 2′-hydroxyls and atoms of neighboring molecules are only observed in the *G*-chimera structure. The 2′-hydroxyl of residue *rG*(1) is positioned at almost equal distances from nitrogen N3 of residue A(15) of a neighboring molecule and O5′ of the adjacent residue C(2) (Figure 9A, Table III). The distances of ~3.2 Å correspond approximately to the sum of the van der Waals radii of the participating oxygens and indicate relatively weak interactions. Since both O5′ and N3 are

Table III: Distances of Intramolecular O2′–Hydrogen Bonds in the Three Chimeric Duplex Molecules[a]

atom 1	atom 2	distance (Å)
	G-Chimera	
O2′ [*rG1*]	O5′ [C2]	3.17
	N3 [A15*]	3.29
	O1′ [C2]	3.88
O2′ [*rG11*]	O5′ [C12]	3.17
	N3 [A15**]	3.29
	O1′ [G12]	3.52
	A-Chimera	
O2′ [*rA5*]	O5′ [T6]	3.27
	W21 [25]	2.56
	O1′ [T6]	3.61
O2′ [*rA15*]	O1′ [T16]	2.75
	Okazaki Fragment	
O2′ [*rG11*]	O1P [*rC12*]	2.84
	W14 [22]	3.19
O2′ [*rC12*]	O1′ [*rG13*]	3.41
O2′ [*rG13*]	O1′ [T14]	3.43

[a] Residues are given in brackets. For the *G*- and *A*-chimeras, all of the distances between 2′- and 1′-oxygens of adjacent riboses have been listed for comparison. Atoms from symmetry-related duplexes are starred.

acceptors, the arrangement may be interpreted as a weak three-centered hydrogen bond. At the other terminal base pair, the pseudosymmetrical 2′-hydroxyl of residue *rG*(11) is hydrogen bonded to N3 of a second neighbor and to the O5′ of residue C(12) (Figure 9B, Table III). The geometries of the hydrogen bonds are almost identical for the two ribose oxygens (Table III). The distances between the 2′- and 1′-oxygens of adjacent residues are much longer in both cases and cannot be regarded as hydrogen bonds.

The environments of the two ribose 2′-hydroxyls in the *A*-chimera structure are quite different from each other. In the first strand, O2′ of residue *rA*(5) forms two hydrogen bonds, a weak one to O5′ of the adjacent residue T(6), and a short one to a water molecule (Figure 10A, Table III). In the other strand, O2′ of residue *rA*(15) forms a hydrogen bond to O1′ of the adjacent residue T(16) (Figure 10B, Table III). As indicated before, there are considerable deviations in the backbone geometries for the two strands. For the other RNA residue, the distance between the ribose oxygen and O1′ of the adjacent sugar is almost 1 Å longer (Table III). The sugar puckers for the two residues are different: In the case of *rA*(5), the ribose adopts a C3′-endo conformation, whereas the conformation of *rA*(15) is C2′-exo.

In the Okazaki fragment, the distances between 2′- and 1′-oxygens of adjacent residues in the case of two of the RNA residues are somewhat shorter than for *G*- and *A*-chimeras (Table III). Nevertheless, the distances of ~3.4 Å indicate that these hydrogen bonds are rather weak. The 2′-hydroxyl of the terminal RNA residue *rG*(11) in the Okazaki fragment is hydrogen bonded to a phosphate oxygen of residue *rC*(12). The three intramolecular hydrogen bonding types present in the hybrid structures are summarized in Figure 11. The ribose of residue *rG*(11) appears to have rotated around a vector defined by atoms C1′ and C3′ (Figure 11A,B). This conformational change is the consequence of rotations around torsions δ (sugar pucker) and ζ (see torsion angles for residue *rG*(1) of the *G*-chimera and residue *rG*(11) of the Okazaki fragment in Table II, sections A and C). The backbone alterations for residue *rA*(15) are apparent when comparing parts B and C of Figure 11. As mentioned previously, the O2′ of residue *rA*(5) in the *A*-chimera forms a hydrogen bond to the adjacent O5′, similar to that in the *G*-chimera depicted in Figure 11B. A comparison of the backbone torsion angles

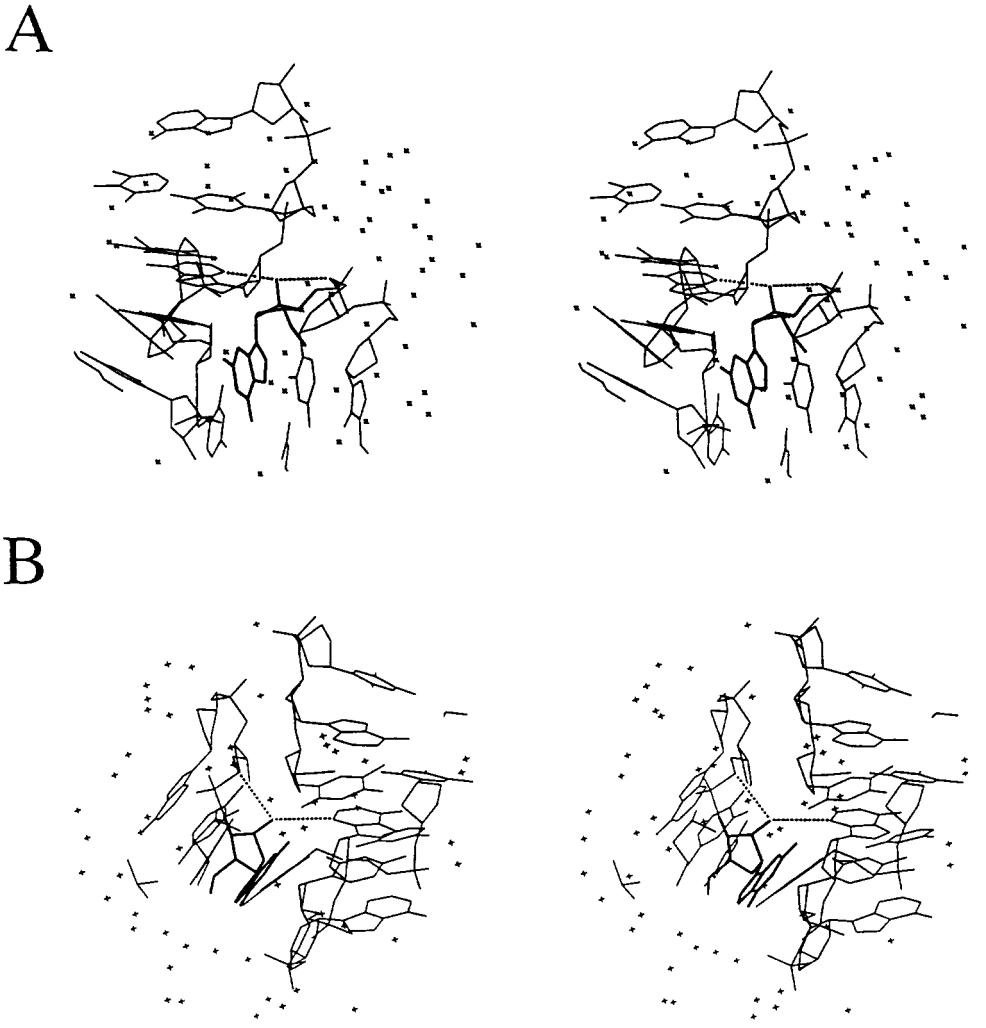

FIGURE 9: Stereo diagrams of the 2′-hydroxyl environments of the RNA residues *rG*(1) (A) and *rG*(11) (B) in the crystal structure of the *G*-chimera. The diameter of the diagrams is 20 Å. RNA residues are bold, and hydrogen bonds are dashed. Water molecules are small crosses.

of deoxyriboses adjacent to RNA residues [T(16) of the *A*-chimera and C(2) of the *G*-chimera] in parts B and C of Figure 11 and in Table II, sections A and B, reveals that the largest deviation occurs between the β torsion angles. Thus, the backbone in A-conformations can undergo subtle conformational alterations, resulting in stabilizing intramolecular hydrogen bonds between ribose 2′-hydroxyls and neighboring backbone atoms.

Crystal Packing. Although the orientations of the duplexes in the crystallographic unit cells are different for the three chimeric duplex structures (Figure 2), their molecular packings have some features in common. The terminal base pairs of each molecule are stacked into the minor grooves of two different neighbors. In turn, two further neighboring molecules have one of their terminal base pairs tucked into its own shallow minor groove. Thus, each duplex has direct lattice contacts to four neighboring molecules.

The packing mode of the *G*-chimera is illustrated in Figure 12, which shows a projection of a layer of molecules along the crystallographic *x*-axis. About six base pairs of the minor groove of each duplex (drawn with thick lines) are covered by neighboring molecules (drawn with thin lines) in this way. Similar stacking interactions between molecules via their minor grooves were also observed with other DNA or RNA sequences which adopt A-type conformations, in either the same or different space groups [e.g., Wang et al. (1982b), Shakked and Kennard (1985), Dock-Bregeon et al. (1989), and Verdaguer et al. (1991)]. Contacts between molecules include hydrogen bonds between deoxyribose atoms and base atoms in the minor groove, as well as interactions between the edges of bases within the minor grooves of two duplexes.

In the crystal lattice of the *A*-chimera, the terminal base pair G(1)·C(20) of a duplex (similar to the molecule drawn with thick lines in the case of the *G*-chimera shown in Figure 12) is stacked on the sugar of residue C(8) from a first neighbor. N2 of G(1) donates in a hydrogen bond to O1′ of the sugar (3.0 Å). At the other end of the duplex, base pair C(10)·G(11) is stacked on the deoxyriboses of residues C(18) and G(19) from a second neighbor. Both terminal residues form two hydrogen bonds into the minor groove of that neighbor. The terminal O3′ of C(10) donates to N3 of residue G(19) (2.3 Å), and O2 of C(10) is located 3.2 Å from N2 of residue G(3) from the same neighbor. N2 of the terminal residue G(11) participates in a three-centered hydrogen bond. It is located 2.3 Å from O2 of residue C(18) and 3.2 Å from O2 of residue T(4), both from the second neighbor. Two additional duplexes (thin lines) contact the minor groove of the duplex (thick lines) at locations which are identical (symmetry related) to the ones which it contacts itself via its own terminal residues. This packing is similar to that of the *G*-chimera, in which the molecules touch at slightly different locations within the minor groove.

In the crystal lattice of the Okazaki fragment, the terminal base pair G(1)·C(20) is stacked on the deoxyriboses of residues A(7) and C(8) from a neighboring duplex. At the other end of the duplex, base pair C(10)·*rG*(11) is stacked on the

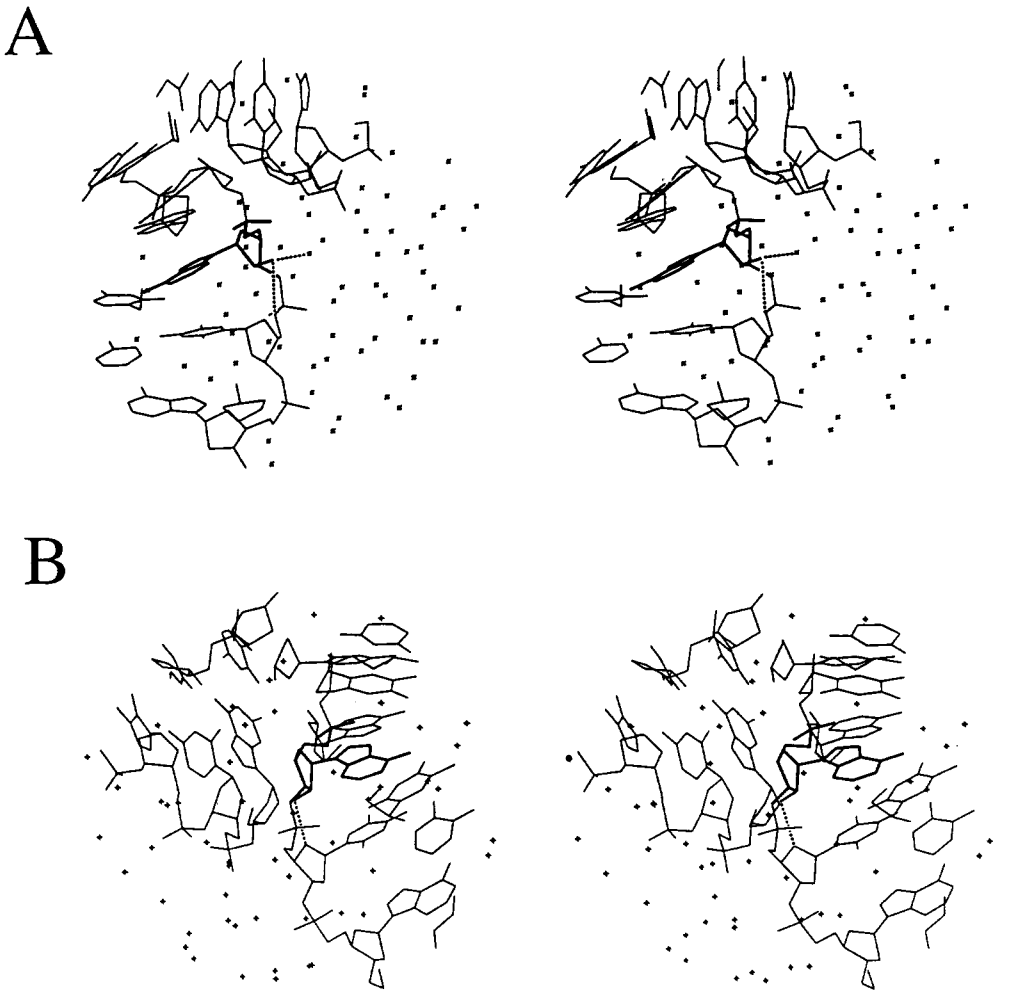

FIGURE 10: Stereo diagrams of the 2′-hydroxyl environments of the RNA residues *rA*(5) (A) and *rA*(15) (B) in the crystal structure of the *A*-chimera. The diameter of the diagrams is 20 Å. RNA residues are bold, and hydrogen bonds are dashed. Water molecules are small crosses.

deoxyribose of residue C(19) from a second neighbor. The shortest contact is between N1 of *rG*(11) and O1′ of the deoxyribose (3.0 Å). The terminal hydroxyl group of residue C(10) forms a hydrogen bond to N2 of residue G(2), located in the minor groove of the same neighbor (2.7 Å).

The packing arrangement in space group $P2_12_12_1$ generates large channels which are filled with solvent molecules (Figure 12). The water contents of the hybrid crystals are similar to those of other A-form crystals (see Table I). In the Okazaki fragment crystal structure there is a spermine molecule lying between chimeric duplexes. This spermine contacts the DNA and several water molecules via its protonated amino and imino nitrogens. The closest contact to the DNA is between N14 and O1′ of residue *rG*(13) (2.5 Å).

DISCUSSION

The overall conformations of both self-complementary DNA–RNA chimeric duplexes and the Okazaki fragment, composed of a chimeric DNA–RNA strand and an all-DNA strand, resemble those of other A-type duplexes (Shakked et al., 1981; Wang et al., 1982a). However, the three structures exhibit considerable variations in their local geometries. The TpA steps in the central parts of the duplexes show relative destacking of bases and a combination of low twist angles with high base rolls. Such perturbations, together with propeller twisting and shearing between bases, result in a substantial difference in the relative lengths of the two hydrogen bonds in A·T base pairs within the TATA section. The O4(T)–N6(A) hydrogen bond is consistently longer (between 0.1 and 0.4 Å) than the N3(T)–N1(A) hydrogen bond (Figure 8).

In the Okazaki fragment, the geometry of the all-DNA duplex d(CCC)·d(GGG) is more regular than that of the d(CGC)·*r*(*GCG*) hybrid duplex at the opposite end of the molecule (Figure 1C). Shearing of bases results in the formation of three-centered hydrogen bonds in the hybrid duplex. Base pairs C(8)·*rG*(13) and A(7)·T(14) at the junction site between the hybrid trimer and the DNA heptamer both show considerable buckle, and the roll between the two base pairs is higher than the average value found for the fragment. The backbones of the hybrid duplexes adopt nonuniform structures, and the torsions of several residues lie outside the conformational ranges normally observed in A-type conformations (Arnott et al., 1976). There are several possible reasons for the hetereogeneity of the A-conformation. The structural pattern observed in the TATA sections of the hybrids is consistent with the geometrical characteristics of such pyrimidine–purine steps in other structures and indicates a sequence dependency of the geometry of A-type duplexes (Shakked & Kennard, 1985). Concerted changes in backbone and glycosyl torsion angles can improve the overlap of bases within and across strands, and the maximization of base stacking is presumably the driving force for local geometrical variations in A-type duplexes.

In B-DNA, deoxyriboses normally adopt the C2′-endo (S) conformation, whereas in A-DNA or A-RNA, the confor-

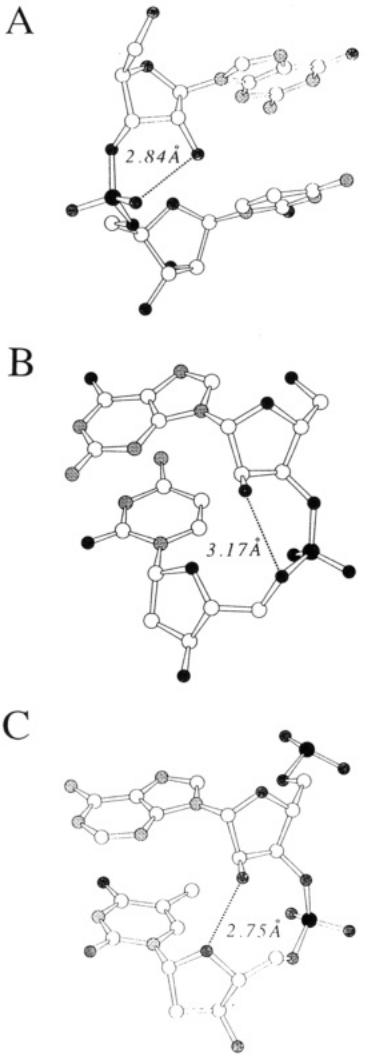

FIGURE 11: Summary of intramolecular hydrogen-bonding types involving 2′-hydroxyls found in the crystal structures of the *G*- and *A*-chimeras and the Okazaki fragment. (A) Hydrogen bond between O2′ of residue *rG*(11) and phosphate oxygen O1P of the adjacent residue *rC*(12) in the Okazaki fragment. (B) Hydrogen bond between O2′ of residue *rG*(1) and O5′ of the adjacent residue C(2) in the *G*-chimera. (C) Hydrogen bond between O2′ of residue *rA*(15) and O1′ of the adjacent residue T(16) in the *A*-chimera. Phosphorus atoms are black, oxygen atoms are hatched, nitrogen atoms are stippled, and hydrogen bonds are dashed.

mation of deoxyriboses or riboses is usually C3′-endo (N). Although the three hybrids belong to the A-conformation family, the puckers of the deoxyriboses and riboses are not restricted to the typical C3′-endo type (Figure 7). In the chimeric duplexes, the different sugar puckers do not lead to significant global changes of the A-conformation. One can therefore conclude that the assignment of sugar conformations alone is probably not sufficient to establish whether the overall conformation of a duplex is A or B. In some cases, the adoption of an alternative sugar conformation in the backbones of the *A*-chimera and the Okazaki fragment is associated with intramolecular interactions of the ribose 2′-hydroxyl groups. Another reason for local geometrical variations in A-type duplexes is crystal-packing effects. The structures of A-DNA octamers were determined in two crystal forms, and the assumed conformations were significantly different in the two environments (Jain & Sundaralingam, 1989; Shakked et al., 1989).

Conformational Influence of the 2′-Hydroxyl Group. Three types of intramolecular hydrogen bonds between 2′-hydroxyls and backbone atoms are observed in the chimeric duplex structures (Figure 11). These are the hydrogen bond to O1′ of the adjacent sugar in a 5′ to 3′ direction, the hydrogen bond to O5′ of the adjacent residue, and the hydrogen bond to one of the phosphate oxygens. In some cases, formation of the hydrogen bond is associated with substantial alterations of the local backbone geometry. This is evident from a comparison of either parts A and B or parts B and C of Figure 11. In the case of the hydrogen bond between O2′ and O1P in the Okazaki fragment (Figure 11A), the ribose appears to have rotated toward the reader around an axis formed by carbons C1′ and C3′. When comparing parts B and C of Figure 11, one notices that the elbow formed by the phosphorus and atoms O5′ and C5′ has swung upward in the structure of the *G*-chimera (Figure 11B), moving O5′ into hydrogen-bonding distance of O2′. In the structure of the *A*-chimera, the O5′ in the elbow is pointing in the opposite direction, resulting in a hydrogen bond between O2′ and O1′.

A number of explanations have been proposed regarding the stabilization of RNA secondary structure and the preference for C3′-endo puckering of riboses in RNA (Saenger, 1984). The relative conformational rigidity may be related to the electronegativity of the substituent at the 2′-position, in which strong electronegativity is associated with a preference for the C3′-endo conformation. Hydrogen bonds between O2′ and O1′ of the adjacent ribose (Seeman et al., 1976) or water-mediated hydrogen bonds between O2′ and phosphate oxygens or base atoms (Rosenberg et al., 1976; Wang et al., 1982a; Westhof et al., 1988) may also contribute to the stabilization of the A-conformation in double-helical RNA.

An analysis of the O2′ environments in the crystal structure of $tRNA^{Phe}$ (excluding intermolecular and water-mediated hydrogen bonds) shows that the same intramolecular types of hydrogen bonds between 2′-hydroxyls and atoms of the backbone that were observed in the chimeric duplex structures are also present in tRNA. Hydrogen-bonding partners and distances of all hydrogen bonds are listed in Table IV. Analyzing how often the different types occur, one notices that the hydrogen bond between O2′ and O5′ is more common than the one between O2′ and O1′. In a number of cases, there are three-centered hydrogen bonds between O2′ and both O1′ and O5′. Both oxygens are good hydrogen-bond acceptors, and hydrogen bonds between either of them and O2′ can stabilize alternative local backbone conformations, resulting in a duplex with an overall A-form helix. A search through the crystal structures in the Cambridge Structural Data Base did not produce any evidence for the role of O5′ as a hydrogen-bond acceptor. This is not surprising, however, since in crystal structures of small molecules, such as mono- or dinucleotides (they are rare in the data base), the charged phosphate oxygens are the dominant hydrogen-bond acceptors (Jeffrey et al., 1985). An analysis of the hydration sites in nucleic acids revealed that the anionic phosphate oxygens are the most hydrated, the sugar O1′ oxygens are intermediately hydrated, and the esterified O3′ and O5′ oxygens in the backbone are the least hydrated (Westhof, 1987). Also, O5′ oxygens are involved in water binding slightly more often in B-DNA than in A- and Z-DNA.

Another notable feature of the hydrogen-bonding geometry in tRNA is the rather long distance between O2′ and O1′ of the adjacent ribose in many cases. This is consistent with the distances of such interactions observed in the chimera structures. One can thus conclude that this hydrogen-bonding type is not the predominant reason for secondary structure stability in duplex RNA. The stabilizing influence of the

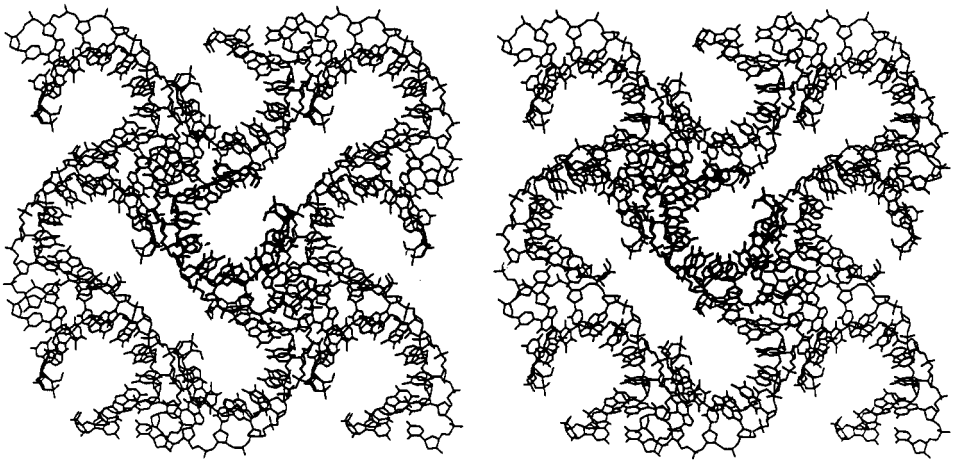

FIGURE 12: Stereo drawing showing intermolecular interactions between chimeric duplexes in the crystal lattice of the *G*-chimera. The terminal base pairs of each duplex (drawn with thick lines) stack into the minor grooves of two neighboring molecules (drawn with thin lines). The terminal base pairs of two further duplexes (thin lines) are stacked into the minor groove of the central molecule (thick lines).

Table IV: Intramolecular Hydrogen Bonds of Ribose 2′-Oxygens in the Crystal Structure of Yeast $tRNA^{Phe}$ [a]

O2′	residue	residue 2	atom	d_1 (Å)	d_2 (Å)	O2′	residue	residue 2	atom	d_1 (Å)	d_2 (Å)
1	pG	2	O1′	2.72	2.72	39	ψrd	40			3.90
2	C	3			3.52	40	m^5C				
3	G	4	O1′	2.87	2.87	41	U	42	O1′	3.14	3.14
4	G	5	O5′	2.79	3.47	42	G	43	O5′	2.92	2.84
5	A	6	O5′	2.65	3.18	43	G	44	O5′	3.28	3.39
6	U	7	O5′	3.07	3.38	44	A	45	O5′	3.13	3.59
7	U	49	O5′	2.84	3.12	45	G				
8	U	21	N1	2.58		46	m^7G				
		46	N2	2.96		47	U	48	O2P	3.14	
9	A	10	N7	2.81				50	O2P	3.13	
		11	N4	3.14		48	C	59	O1′	2.96	2.96
10	m^2G					49	m^5C				
11	C	12			3.81	50	U	51			3.36
12	U	13	O5′	3.14	3.89	51	G	52	O5′	2.94	3.11
13	C	14	O5′	3.25		52	U	53	O1′	3.25	3.25
14	A					53	G	54			3.77
15	G					54	T				
16	H^2U					55	ψrd	57	N7	2.87	
17	H^2U	19	O1P	3.01		56	C	57			3.75
18	G	57	N1	2.89		57	G				
19	G					58	m^1A	60	O1P	2.68	
20	G					59	U	48	O2′	2.96	
21	A	22	O1P	2.54				60	O5′	2.86	3.99
22	G	23			3.61	60	C				
23	A	24	O1′	3.13	3.13	61	C	62	O5′	2.77	3.22
24	G	25			3.84	62	A	63			3.41
25	C	26	O5′	2.85	3.45	63	C	64	O1′	3.15	3.15
26	m^2G	27	O5′	2.84	3.93	64	A	65	O5′	2.91	3.38
27	C	28			3.37	65	G	66			3.57
28	C	29	O1′	3.24	3.24	66	A	67	O5′	2.86	2.97
29	A	30	O5′	2.64	3.47	67	A	68	O1′	3.25	3.25
30	G	31	O5′	2.85	3.30	68	U	69	O5′	3.13	3.06
31	A	32	O5′	3.23	3.94	69	U	70			3.42
32	OmC					70	C	71	O5′	2.68	2.93
33	U	35	N7	2.43		71	G	72			3.25
34	OmG					72	C	73	O5′	3.21	
35	A	36	O1′	2.61	2.61	73	A	74			3.97
36	A					74	C				
37	Y	38			3.62	75	C				
38	A	39	O1′	2.90	2.90	76	A				

[a] Quigley et al., (1975); Rich and RajBhandary (1976). Intramolecular hydrogen bonds mediated by water molecules were excluded. The table lists distances d_1 of hydrogen bonds between the O2′ of one residue and one or more atoms from neighboring residues (residue 2) which are shorter than 3.3 Å. The distance between O2′ and O1′ of the adjacent residue in a 5′ to 3′ direction (usually, the O2′ residue is n, and residue 2 is $n + 1$) is included as d_2 if it is shorter than 4 Å. In cases where O2′ forms a bifurcated hydrogen bond to O1′ and a second atom, the distance to the former is listed as d_2 and the distance to the latter is listed as d_1.

ribose 2′-hydroxyl group seems to be based on various possible interactions that depend on the local environment. The unusual hydrogen bond between O2′ and one of the phosphate oxygens from the adjacent residue in the Okazaki fragment can probably be attributed to the terminal location of the ribose residue. However, there are several different interactions between O2′ and phosphate oxygens in the structure of $tRNA^{Phe}$, and such interactions can stabilize hairpin conformations. In the case of residues 20, 21, and 22 (Table IV), which are located at the end of the D stem, one of the

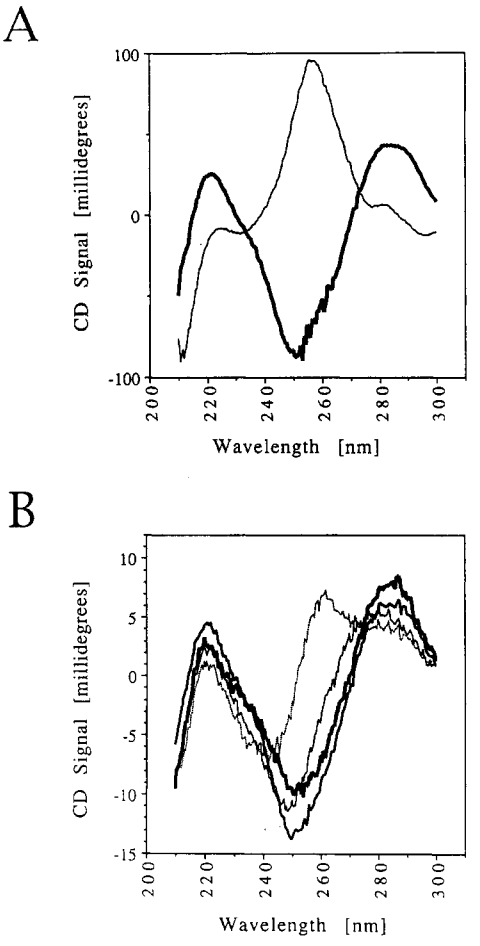

FIGURE 13: (A) CD spectra of an all-DNA decamer duplex with the sequence d(GCGTATACGC) (thick line) and an all-RNA duplex with the identical sequence. (B) CD spectra for the *G*-chimera (thin line), the *A*-chimera (medium line), the Okazaki fragment (dashed line), and the all-DNA decamer duplex (thick line).

phosphate oxygens of residue 22 is hydrogen bonded to O2′ of residue 21 (2.54 Å). O2′ of residue 22 is located 3.61 Å from O1′ of the adjacent residue, and both residues are part of a regular A-form duplex. Residue 20 is situated in the D loop, and its ribose is rotated away, resulting in a longer distance between its O2′ and O1′ of the adjacent residue 21 (4 Å). The A-conformation adopted by the hybrids thus allows enough geometrical variability for the 2′-hydroxyls of the ribose residues to interact with different backbone atoms in a stabilizing manner.

Solution Structure of the Chimeric Duplexes and the Conformation of the All-DNA Duplex. To analyze the conformations of the hybrids in solution, CD spectra were recorded for the three chimeras as well as for all-DNA and all-RNA duplexes with sequences identical to those of the self-complementary *G*- and *A*-chimeras. Figure 13A shows a comparison of the spectra of the all-DNA and all-RNA duplexes. The spectrum of the DNA duplex is representative of a B-type conformation with a long-wavelength maximum around 280 nm and a short-wavelength minimum around 250 nm. The spectrum of the RNA duplex is representative of an A-type conformation with a long-wavelength maximum around 250 nm and a shallow minimum around 230 nm.

The chimera spectra and the spectrum of the all-DNA duplex are shown in Figure 13B. In the *G*-chimera and Okazaki fragment spectra, the maxima and minima have shifted toward shorter wavelengths relative to the signals of the B-type spectrum of the DNA duplex. The spectrum of the *A*-chimera is qualitatively similar to the spectrum of the DNA, but it differs quantitatively. The different conformational influences of RNA residues located at the ends of a duplex (*G*-chimera) and in the middle of a duplex (*A*-chimera) may be the reason for the deviations between the CD spectra of the two self-complementary chimeras. The spectrum of the Okazaki fragment (Figure 13B) shares features of the spectra of both DNA and RNA (Figure 13A) in terms of the shape of the CD signal. The positions of the maximum and the minimum are similar to those in the RNA spectrum. However, in contrast to the spectra of DNA and RNA, the magnitudes of the minimum and the maximum are almost equal in the spectrum of the Okazaki fragment. These spectra do not suggest pure A-conformations of the chimeras under the measuring conditions used. More importantly, though, the conformational influence of the RNA residue is evident in all three cases. Thus, single RNA residues in self-complementary DNA–RNA chimeras can certainly cause alterations of the helix conformation. However, such interpretations are based on the assumption that the all-DNA duplex adopts a B-type conformation.

Table V: Sequences of DNA Oligonucleotides Adopting A-Type Conformation in the Crystal[a]

sequence	reference
d(GGTATACC)	Shakked et al. (1981)
d(*CCGG)	Conner et al. (1982)
d(GGCCGGCC)	Wang et al. (1982b)
d(GGGGCCCC)	McCall et al. (1985)
d(GGATGGGAG)/ d(CTCCCATCC)	McCall et al. (1986)
d(CCCCGGGG)	Haran et al. (1987)
d(GCCCGGGC)	Heinemann et al. (1987)
d(GGGATCCC)	Lauble et al. (1988)
d(GGGCGCCC)	Rabinovich et al. (1988)
d(GTGTACAC)	Jain et al. (1989b)
d(ACCGGCCGGT)	Frederick et al. (1989)
d(GTACGTAC)	Takusagawa (1990)
d(CCCCCGCGGGGG)	Verdaguer et al. (1991)

[a] *C is iodo^{5}C.

There are several arguments that support this assumption. From earlier NMR experiments, it was concluded that the DNA sequence d(GCGTATACGC) has a normal B-type structure in solution (Mellema et al., 1983). From fiber diffraction studies, it is known that alternating purine–pyrimidine sequences (see Figure 1) normally adopt B-type geometry (Arnott et al., 1975). The decamer has sequence characteristics which are distinct from those of oligonucleotides adopting the A-conformation in the crystalline state. Table V lists the sequences of all oligonucleotides which crystallize as A-form duplexes. Except for two sequences (Jain et al., 1989; Takusagawa, 1990), all of them are composed of short guanosine stretches which alternate with short stretches of cytidines, and sequences starting with either a purine or a pyrimidine residue are represented. Both of the above oligonucleotides with purines and pyrimidines alternating are eight nucleotides long. The sequence of the only decamer which adopts an A-conformation is closely related to those of some octamers. Although there is no obvious reason to associate the sequence d(GCGTATACGC) with the adoption of an A-type conformation, an attempt was made to grow single crystals of the DNA decamer.

Numerous crystallization conditions were tested, and among others, magnesium concentration and pH were varied over large ranges. However, the best crystals were obtained under conditions which were quite similar to those used for the

chimeras.[2] The morphologies of the DNA and chimera crystals are different, and the DNA crystals are much more sensitive to temperature than those of the chimeras (data not shown). The cell constants of the DNA crystals are $a = b =$ 27.3 Å and $c = 132.2$ Å, and the crystal system is hexagonal. The crystals diffract only weakly, and the data obtained is not sufficient for an analysis of the structure. Nevertheless, if the A-type conformation were an intrinsic property of the above DNA sequence, one would expect it to adopt a similar overall conformation in either the same or another space group. In addition, the 2′-hydroxyl groups in the three chimeric duplex structures are predominantly engaged in intramolecular hydrogen bonds and are therefore of minor importance in the stabilization of the lattice. The observation that the chimeric duplexes adopt A-type conformations in the crystal, together with their partial A character in solution, can thus be attributed to the ribose residues. More relevant than a speculation about the extent of RNA secondary structure propagation along a DNA duplex is the experimental finding that a single ribose residue in a DNA strand can nucleate an A-type conformation, which then may well be stabilized locally through other influences, such as sequence, solvent conditions, or packing forces.

Biological Implications. The chimeric duplex structures constitute three further examples of A-type duplexes which incorporate a TATA portion in their sequence. The particular geometry of the TpA steps in the chimeras is consistent with the geometries of short TA stretches in an octamer (Shakked et al., 1983) and in an earlier chimeric duplex decamer (Wang et al., 1982a). TA stretches are found in the promotor regions of both prokaryotic and eukaryotic genes and form part of the binding site for the RNA polymerase prior to unwinding of the DNA during transcription. One is tempted to assume that the DNA at such locations might adopt an A-like conformation, which could be recognized by the polymerase. Geometrical features observed at TpA steps, such as unwinding, partial unstacking of bases, and elongation of Watson–Crick-type hydrogen bonds, might facilitate the melting of the DNA required for transcription.

The recognition of double-helical B-DNA by proteins involves mainly the functional groups of bases in the wide major groove. However, the recognition of duplex RNA must involve other mechanisms, since the edges of bases are inaccessible in the deep and narrow major groove of the A-conformation. Probing of bases might occur at the ends of double-helical regions, where the major groove is relatively open, or at locations where the major groove is widened, such as single- or multiple-bulge sites. In addition, the minor groove contains a restricted amount of information, and recognition may involve single-stranded regions [reviewed in Egli (1992)]. Thus, the arrangement of the 2′-hydroxyl group of the terminal ribose residue in the Okazaki fragment structure provides a unique function in the major groove, which can be probed at the end of a duplex. A similar situation is also observed at the junction between the D stem and the D loop in the crystal structure of $tRNA^{Phe}$. The other 2′-hydroxyls in the Okazaki fragment and in both self-complementary chimeras are located at the rims of the minor groove.

Therefore, enzymes such as RNase H and reverse transcriptase must probe the minor groove for 2′-hydroxyls to differentiate between the A-form of double-stranded RNA, DNA, and DNA·RNA hybrids. From proposed models of the complex of a hybrid duplex and RNase H (Yang et al., 1990; Nakamura et al., 1991), there are several contacts between polar side chains of the protein and phosphate oxygens and 2′-hydroxyls from the ribonucleotide strand of the hybrid duplex. However, between the deoxyribonucleotide strand and the enzyme, steric interactions seem to be dominant. Thus, the models can explain a number of experimental observations regarding the cleavage efficiency of RNase H. The RNA strand is not cleaved in chimeras composed of a deoxyribonucleotide strand and a ribonucleotide strand with methylated 2′-oxygens. Moreover, cleavage efficiency is lower when the RNA strand is paired to a 2′-*O*-methyl nucleotide strand, which can be explained by steric clashes between the methyl groups and the enzyme (Inoue et al., 1987). The important role of the 2′-hydroxyls in the minor groove in recognition is supported by studies using chemically modified oligonucleotides, which suggest that the RNase H enzyme does not interact with the major groove (Wyatt & Walker, 1989).

The crystal structures of the complexes between HIV-1 reverse transcriptase and a duplex DNA template–primer (Arnold et al., 1992) and an inhibitor (Kohlstaedt et al., 1992) have recently been reported. In the DNA complex, the DNA binds in a groove on the surface of the enzyme. However, much of the double-helical density can be fit with either A- or B-form DNA due to the restricted resolution. The elucidation of the details of the recognition process between these enzymes and DNA·RNA hybrids awaits determination of the high-resolution structure and the crystallization of a complex between the enzymes and the real substrate.

A recent report (Musier-Forsyth & Schimmel, 1992) on interactions between *E. coli* $tRNA^{Ala}$ synthetase and chimeric DNA–RNA double-stranded substrates has indicated the requirement for 2′-hydroxyl groups in the minor groove at the recognition site. In fact, a nonamer chimeric duplex containing 3 DNA·RNA base pairs is a substrate for the synthetase enzyme, while an all-DNA duplex is not. Although the minimally substituted chimera was a poorer substrate than an all-RNA duplex, we may speculate that the chimeric duplex does adopt an A-form duplex structure at least some of the time and that it is this form which is recognized, along with the necessary 2′-hydroxyl groups, by the synthetase enzyme.

Finally, self-cleavage of RNA in the "hammerhead" ribozyme is associated with a small domain of RNA containing three duplex stems and a large single-stranded catalytic core. Two of the duplex stems comprise the enzyme fragment annealing to its substrate. The incorporation of deoxyribonucleotides into synthetic substrate and ribozyme fragments was used to determine the role of ribonucleotides in catalysis (Perreault et al., 1991; Yang et al., 1992). These studies showed that both substrate RNA and enzymatic fragment are surprisingly tolerant of extensive deoxyribonucleotide substitutions. In the case where a 35-mer chimeric enzyme containing only four ribonucleotides is annealed to a 14-mer RNA substrate, catalytic cleavage of the substrate still occurs. In this complex there are two DNA·RNA hybrid duplexes, and 7 of 11 of the single-stranded nucleotides in the catalytic core are deoxyribonucleotides. In light of our observation that only a small number of ribonucleotides are necessary to maintain the A-conformation in the duplex regions, the activity of these chimeric enzymes may be attributed to both the maintenance of A-form duplexes in two of the stems and the

[2] Crystals were grown at 4 °C in sitting drops by using the vapor diffusion technique. The crystallization mother liquor initially contained 1.7 mM DNA (single strand), 30 mM sodium cacodylate buffer (pH 7.5), 8 mM magnesium chloride, and 9 mM spermine tetrachloride. The sitting drops were equilibrated against a reservoir of 20 mL of 20% (v/v) 2-methyl-2,4-pentanediol. Crystals began to appear within 2 weeks and grew to a typical size of $0.2 \times 0.2 \times 0.1$ mm^3.

presence of specific 2′-hydroxyls in the catalytic core.

ACKNOWLEDGMENT

We would like to thank the Sauer group, especially Ms. Susan Marqusee, for help with the CD spectra and Ms. Lynn Albers for help with the refinement of the *A*-chimera as part of her undergraduate research project.

REFERENCES

Arnold, E., Jacobo-Molina, A., Nanni, R. G., Williams, R. L., Lu, X., Ding, J., Clark, A. D., Jr., Zhang, A., Ferris, A. L., Clark, P., Hizi, A., & Hughes, S. H. (1992) *Nature 357*, 85–89.

Arnott, S., Chandrasekaran, R., & Selsing, E. (1975) in *Structure and Conformation of Nucleic Acids and Protein–Nucleic Acid Interactions* (Sundaralingam, M., & Rao, S. T., Eds.) pp 577–596, University Park Press, Baltimore.

Arnott, S., Smith, P. J. C., & Chandrasekaran, R. (1976) in *CRC Handbook of Biochemistry and Molecular Biology* (Fasman, G. D., Ed.) 3rd ed., Vol. 2, pp 411–422, CRC Press, Cleveland, OH.

Arnott, S., Chandrasekaran, R., Millane, R. P., & Park, H.-S. (1986) *J. Mol. Biol. 188*, 631–640.

Benevides, J. M., & Thomas, G. J., Jr. (1988) *Biochemistry 27*, 3868–3873.

Benevides, J. M., Wang, A. H.-J., Rich, A., Kyogoku, Y., van der Marel, G. A., van Boom, J. H., & Thomas, G. J., Jr. (1986) *Biochemistry 25*, 41–50.

Chou, S.-H., Flynn, P., & Reid, B. (1989) *Biochemistry 28*, 2435–2443.

Chou, S.-H., Flynn, P., Wang, A., & Reid, B. (1991) *Biochemistry 30*, 5248–5257.

Conner, B. N., Takano, T., Tanaka, S., Itakura, K., & Dickerson, R. E. (1982) *Nature 295*, 294–299.

Crouch, R. J., & Dirksen, M.-L. (1982) in *Nuclease* (Linn, S. M., & Roberts, R. J., Eds.) pp 211–241, Cold Spring Harbor Laboratory Press, Cold Spring Harbor, NY.

Dickerson, R. E., et al. (1989) *Nucleic Acids Res. 17*, 1797–1803.

Dobler, M. (1992) MoMo (color version 1.4), ETH Zürich.

Dock-Bregeon, A. C., Chevrier, B., Podjarny, A., Johnson, J. E., deBear, J. S., Gough, G. R., Gilham, P. T., & Moras, D. (1989) *J. Mol. Biol. 209*, 459–474.

Egli, M. (1992) in *Structure Correlation* (Dunitz, J. D., & Bürgi, H.-B., Eds.) VCH Publishers, Weinheim (in press).

Egli, M., Usman, N., Zhang, S., & Rich, A. (1992) *Proc. Natl. Acad. Sci. U.S.A. 89*, 534–538.

Evans, D. B., Brawn, K., Deibel, M. R., Jr., Tarpley, W. G., & Sharma, S. K. (1991) *J. Biol. Chem. 266*, 20583–20585.

Frederick, C. A., Quigley, G. J., Teng, M.-K., Coll, M., van der Marel, G. A., van Boom, J. H., Rich, A., & Wang, A. H.-J. (1989) *Eur. J. Biochem. 181*, 295–307.

Fujii, S., Matsui, S., Tomita, K., Orita, M., Tanaka, T., & Uesugi, S. (1989) *Nucleic Acids Symp. Ser. 21*, 67–68.

Goff, S. (1990) *J. Acquired Immune Defic. Syndr. 3*, 817–831.

Gupta, G., Sarma, M. H., & Sarma, R. H. (1985) *J. Mol. Biol. 186*, 463–469.

Hansen, J., Schulze, T., Mellert, W., & Moelling, K. (1988) *EMBO J. 7*, 239–243.

Happ, C. S., Happ, E., Clore, G. M., & Gronenborn, A. M. (1988) *FEBS Lett. 236*, 62–70.

Haran, T. E., Shakked, Z., Wang, A. H.-J., & Rich, A. (1987) *J. Biomol. Struct. Dyn. 5*, 199–217.

Heinemann, U., Lauble, H., Frank, R., & Blöcker, H. (1987) *Nucleic Acids Res. 15*, 9531–9550.

Hendrickson, W. A., & Konnert, J. H. (1981) in *Biomolecular Structure, Conformation, Function and Evolution* (Srinivasan, R., Ed.) pp 43–57, Pergamon, Oxford.

Hirshfeld, F. L. (1968) *Acta Crystallogr. A24*, 301–311.

Hu, W.-S., & Temin, H. M. (1990) *Science 250*, 1227–1233.

Huber, H. E., & Richardson, C. C. (1990) *J. Biol. Chem. 265*, 10565–10573.

Inoue, H., Hayase, Y., Iwai, S., & Ohtsuka, E. (1987) *FEBS Lett. 215*, 327–330.

Jain, S., & Sundaralingam, M. (1989) *J. Biol. Chem. 264*, 12780–12784.

Jain, S., Zon, G., & Sundaralingam, M. (1989) *Biochemistry 28*, 2360–2364.

Jeffrey, G. A., Maluszynska, H., & Mitra, J. (1985) *Int. J. Biol. Macromol. 7*, 336–348.

Johnson, M. S., McCure, M. A., Feng, D. F., Gray, J., & Doolittle, R. (1986) *Proc. Natl. Acad. Sci. U.S.A. 83*, 7648–7652.

Jones, T. A. (1978) *J. Appl. Crystallogr. 11*, 268–272.

Kabsch, W. (1978) *Acta Crystallogr. A34*, 827–828.

Katahira, M., Lee, S. J., Kobayashi, Y., Sugeta, H., Kyogoku, Y., Iwai, S., Ohtsuka, E., Benevides, J. M., & Thomas, G. J., Jr. (1990) *J. Am. Chem. Soc. 112*, 4508–4512.

Kohlstaedt, L. A., Wang, J., Friedman, J. M., Rice, P. A., & Steitz, T. A. (1992) *Science 256*, 1783–1790.

Kornberg, A. (1974) *DNA Synthesis*, p 367, Freeman, San Francisco.

Lauble, H., Frank, R., Blöcker, H., & Heinemann, U. (1988) *Nucleic Acids Res. 16*, 7799–7816.

McCall, M., Brown, T., & Kennard, O. (1985) *J. Mol. Biol. 183*, 385–396.

McCall, M., Brown, T., Hunter, W. N., & Kennard, O. (1986) *Nature 322*, 661–664.

Mellema, J.-R., Haasnoot, C. A. G., van der Marel, G. A., Wille, G., van Boeckel, C. A. A., van Boom, J. H., & Altona, C. (1983) *Nucleic Acids Res. 11*, 5717–5738.

Milman, G., Langridge, R., & Chamberlin, M. J. (1967) *Proc. Natl. Acad. Sci. U.S.A. 57*, 1804–1810.

Mitsuya, H., & Broder, S. (1987) *Nature 325*, 773–778.

Musier-Forsyth, K., & Schimmel, P. R. (1992) *Nature 357*, 513–515.

Nakamura, H., Oda, Y., Iwai, S., Inoue, H., Ohtsuka, E., Kanaya, S., Kimura, S., Katsuda, C., Katayanagi, K., Morikawa, K., Miyashiro, H., & Ikehara, M. (1991) *Proc. Natl. Acad. Sci. U.S.A. 88*, 11535–11539.

North, A. C. T., Phillips, D., & Matthews, F. S. (1968) *Acta Crystallogr. A24*, 351–359.

Ogawa, T., & Okazaki, T. A. (1980) *Annu. Rev. Biochem. 49*, 421–457.

Okazaki, R., Okazaki, T., Sakabe, K., & Sugimoto, K. (1967) *Jpn. J. Med. Sci. Biol. 20*, 255–260.

Okazaki, R., Okazaki, T., Sakabe, K., Sugimoto, K., & Sugino, A. (1968) *Proc. Natl. Acad. Sci. U.S.A. 59*, 598–605.

Omer, C. A., & Faras, A. J. (1982) *Cell 30*, 797–805.

Panganiban, A. T., & Fiore, D. (1988) *Science 241*, 1064–1069.

Perreault, J.-P., Labuda, D., Usman, N., Yang, J.-H., & Cedergren, R. J. (1991) *Biochemistry 30*, 4020–4025.

Quigley, G. J., Wang, A. H.-J., Seeman, N. C., Suddath, F. L., Rich, A., Sussman, J. L., & Kim, S. H. (1975) *Proc. Natl. Acad. Sci. U.S.A. 72*, 4866–4870.

Quigley, G. J., Teeter, M. M., & Rich, A. (1978) *Proc. Natl. Acad. Sci. U.S.A. 75*, 64–68.

Rabinovich, D., & Shakked, Z. (1984) *Acta Crystallogr. A40*, 195–200.

Rabinovich, D., Haran, T., Eisenstein, M., & Shakked, Z. (1988) *J. Mol. Biol. 200*, 151–161.

Rich, A. (1960) *Proc. Natl. Acad. Sci. U.S.A. 46*, 1044–1053.

Rich, A., & RajBhandary, U. L. (1976) *Annu. Rev. Biochem. 45*, 805–860.

Rosenberg, J. M., Seeman, N. C., Day, R. O., & Rich, A. (1976) *J. Mol. Biol. 104*, 145–167.

Saenger, W. (1984) *Principles of Nucleic Acid Structure*, 1st ed., pp 64–68, Springer-Verlag, New York.

Sawai, Y., & Tsukada, K. (1983) *Biochem. Biophys. Res. Commun. 110*, 470–476.

Schatz, O., Cromme, F., Gruninger-Leitch, R., & LeGrice, S. F. J. (1989) *FEBS Lett. 257*, 311–314.

Seeman, N. C., Rosenberg, J. M., Suddath, F. L., Kim, J. J. P., & Rich, A. (1976) *J. Mol. Biol. 104*, 109–144.
Selsing, E., Wells, R. D., Early, T. A., & Kearns, D. R. (1978) *Nature 275*, 249–250.
Selsing, E., Wells, R. D., Alden, C. J., & Arnott, S. (1979) *J. Biol. Chem. 254*, 5417–5422.
Shakked, Z., & Kennard, O. (1985) in *Biological Macromolecules and Assemblies: Volume 2—Nucleic Acids and Interactive Proteins* (Jurnak, F. A., & McPherson, A., Eds.) pp 1–36, Wiley, New York.
Shakked, Z., Rabinovich, D., Cruse, W. B. T., Egert, E., Kennard, O., Sala, G., Salisbury, S. A., & Viswamitra, M. A. (1981) *Proc. R. Soc. London B213*, 479–487.
Shakked, Z., Rabinovich, D., Kennard, O., Cruse, W. B. T., Salisbury, S. A., & Viswamitra, M. A. (1983) *J. Mol. Biol. 166*, 183–201.
Shakked, Z., Guerstein-Guzikevich, G., Eisenstein, M., Frolow, F., & Rabinovich, D. (1989) *Nature 342*, 456–459.
Shindo, H., & Matsumoto, U. (1984) *J. Biol. Chem. 259*, 8682–8684.
Takusagawa, F. (1990) *J. Biomol. Struct. Dyn. 7*, 795–809.
Tisdale, M., Erl, P., Larder, B. A., Purifoy, D. J. M., Darby, G., & Powell, K. L. (1988) *J. Virol. 62*, 3662–3667.
Usman, N., Egli, M., & Rich, A. (1992) *Nucleic Acids Res. 20*, 6695–6699.
Verdaguer, N., Aymami, J., Fernández-Forner, D., Fita, I., Coll, M., Huynh-Dinh, T., Igolen, J., & Subirana, J. A. (1991) *J. Mol. Biol. 221*, 623–635.
Wang, A. H.-J., Fujii, S., van Boom, J. H., van der Marel, G. A., van Boeckel, S. A. A., & Rich, A. (1982a) *Nature 299*, 601–604.
Wang, A. H.-J., Fujii, S., van Boom, J. H., & Rich, A. (1982b) *Proc. Natl. Acad. Sci. U.S.A. 79*, 3968–3972.
Westhof, E. (1987) *Int. J. Biol. Macromol. 9*, 186–192.
Westhof, E., Dumas, P., & Moras, D. (1988) *Biochimie 70*, 145–165.
Wyatt, J. R., & Walker, G. T. (1989) *Nucleic Acids Res. 17*, 7833–7842.
Yanagi, K., Privé, G. G., & Dickerson, R. E. (1990) *J. Mol. Biol. 217*, 201–214.
Yang, J.-H., Usman, N., Chartrand, P., & Cedergren, R. J. (1992) *Biochemistry 31*, 5005–5009.
Yang, W., Hendrickson, W. A., Crouch, R. J., & Satow, Y. (1990) *Science 249*, 1398–1405.
Zimmerman, S. B., & Pheiffer, B. H. (1981) *Proc. Natl. Acad. Sci. U.S.A. 78*, 78–82.